THE HONG KONG
POLYTECHNIC UNIVERSITY
香港理工大學
Pao Yue-kong Library
包玉剛圖書館

Copyright Undertaking

Pao Yue-kong Library, The Hong Kong Polytechnic University, Hung Hom, Kowloon, Hong Kong

http://www.lib.polyu.edu.hk

FABRICATION OF SINGLE CRYSTAL BASED

PHASED ARRAY MEDICAL IMAGING

ULTRASONIC TRANSDUCERS

LI HENG

M. PHIL.

THE HONG KONG POLYTECHNIC UNIVERSITY

2008

THE HONG KONG POLYTECHNIC UNIVERSITY

THE DEPARTMENT OF APPLIED PHYSICS

FABRICATION OF SINGLE CRYSTAL BASED PHASED ARRAY MEDICAL IMAGING ULTRASONIC TRANSDUCERS

SUBMITTED BY

LI HENG

A THESIS SUBMITTED IN PARTIAL FULFILMENT

OF THE REQUIREMENTS FOR THE DEGREE OF

MASTER OF PHILOSOPHY IN PHYSICS

DECEMBER 2007

CERTIFICATE OF ORIGINALITY

I hereby declare that this thesis is my own work and that, to the best of my knowledge and belief, it reproduces no material previously published or written nor material which has been accepted for the award of any other degree or diploma, except where due acknowledgement has been made in the text.

_____

LI Heng

ABSTRACT

Ultrasound imaging is one of the most used methods for medical diagnostics. Conventional PZT transducers usually can only give a -6dB bandwidth of about 60 - 70%, which is not wide enough for second harmonic imaging. Relaxor-based ferroelectric single crystal, $Pb(Mg_{1/3}Nb_{2/3})O_3$-$xPbTiO_3$ (PMN-PT), is receiving great deal of attention for application in medical imaging ultrasonic transducers because of its high piezoelectric coefficient and electromechanical coupling factor. It has been demonstrated that the PMN-PT single crystal phased array transducers have a wider bandwidth (>100% at -6dB), higher sensitivity and better resolution than conventional transducers made of PZT. In this thesis, development of PMN-PT single crystal phased array transducer with wide bandwidth and high sensitivity is carried out.

PMN-28%PT single crystal oriented along <001> direction is selected to fabricate the phased-array transducer. Array elements are spaced at 0.26 mm with a center frequency around 3 MHz. A KLM model based PiezoCAD simulation was used to help the acoustic design of the transducer, where the effect of the matching layers with different thicknesses and acoustic impedances, the effect of backing materials with different acoustic impedances, and also the effect of electromechanical coupling factor of driving material are studied. Based on the simulation results, two PMN-PT phased

array transducers, with $\lambda/4$ and $\lambda/8$ matching layers, were fabricated. Both transducers show 90% above bandwidth, which is a big increase compared to the conventional PZT phased array transducers (about 70%). The substitution of the PZT ceramic with PMN-PT single crystal with higher electromechanical coupling factor, as the active element in ultrasound transducer, improves the transducer performance. Compared to the well-accepted double quarter wavelength matching system, the novel double $\lambda/8$ matching scheme also shows the trend to further improve the bandwidth of the transducer from my research.

Because of the relatively lower sound velocity of PMN-PT single crystal compared to PZT, the aspect ratio becomes a problem when using PMN-PT to substitute PZT. The 1-3 composite may solve this problem by bringing much high aspect ratio and better coupling factor. In order to further increase the bandwidth, some unique designed transducer structure and process are also tackled in my work. A new transducer with 1-3 composite PMN-PT active elements will be developed in the future study.

THE HONG KONG POLYTECHNIC UNIVERSITY

PUBLICATIONS

H. Li, J.Y. Dai, Y.C. Li, Q.F. Zhou, S.T. Lau, "A 3.8 MHz PHASED ARRAY ULTRASONIC PROBE USING PMN-PT SINGLE CRYSTAL WITH 1/8 MATCHING LAYERS", *submitted to Applied Physics.*

ACKNOWLEDGEMENTS

I would like to express my appreciation to my supervisor Dr. J.Y. Dai for his constant support, valuable suggestions and guidance throughout the period of this study. Grateful acknowledgement is made to my supervisors in the attachment program in the University of Southern California, Prof. K.K. Shung and Dr. Q.F. Zhou for their supports and encouragement. I would also like to thank Prof. H.L.W. Chan for her valuable suggestions, and our cooperator in Anke.co.,ltd, Mr. Y.C. LEE for his supports and suggestions in my research.

Thanks are also due to Dr. J. Pen and Dr. S.T. Lau for their assistance in transducer fabrications, Dr. P.F. Lee, Mr. X. Zhao, Mr. K.S. Wong, Miss. C.K. Cheng, Mr. K. L. Jim, Mr. W. K. Tan, Mr. J. Liu for their kind help and encouragement.

Finally, I wish to thank my family and all my friends for their support in my two years' study.

TABLE OF CONTENTS

LIST OF FIGURES

LIST OF TABLES

CHAPTER 1

INTRODUCTION

1.1   Background

Ultrasound diagnostics is very important in medicine and is now taking its place along with X-ray, computed tomography (CT), magnetic resonance imaging (MRI) and nuclear medicine as an important diagnostic tool. Every day in thousands of hospitals and medical centers around the word, ultrasound is in routine clinical use in diverse body regions such as the brain, heart, liver, kidney, fetal and reproductive systems [Erikson et. al, 1974]. Ultrasound is an ideal diagnostic tool in many ways. First, ultrasonic scanners are far less expensive than both CT and MRI scanners. Second, ultrasound is capable of producing real time images of moving tissues, such as in the heart, making it the best choice for applications where real time image display is essential for diagnosis. Third, ultrasound is the only imaging modality considered non-invasive at the power levels used by imaging scanners. Fourth, ultrasound can be

used to obtain other physiological data such as blood flow to a tissue or organ. And fifth,

ultrasound is more portable than other imaging modalities; very sophisticated fully

portable ultrasound scanners are currently available, for example, the Sonosite 180Plus

(Sonosite Inc., Bothell, WA) [Cannata, 2004].

The interaction between ultrasound and living systems has been studied since the

1820's. The discovery of the piezoelectric effect and its utilization in the construction of

high frequency mechanical vibration sources provides the basis for this work. During

the 1940's and 1950's, ultrasound was in a rather slow evolutionary period. In the

1960's, an ever-increasing number of physicians began to accept ultrasound and to use

this modality in the clinic. In the 1970's people witnessed the widespread use of

ultrasound, as well as the development of new and innovative techniques. Now, the

development of the piezoelectric materials and signal process technology is bringing the

ultrasound imaging technology to the overwhelming status in medical diagnostics.   No

harmful electromagnetic radiation, cost effective, real time imaging ability, better

differentiation of soft tissue, and portable instrumentation makes ultrasound diagnosis

still outstanding the various diagnostic methods today.

1.2   Ultrasound Transducer Structure and Working

Mechanism

Ultrasound waves are generated and detected by transducers; when coupled to tissue, a transducer generates waves that propagates through and reflecting off of internal structures of human body. Using modern electronics, the delay in time and amplitude of a reflected echo returning to the transducer is measured. With knowledge of the speed of sound in the tissue, the distance to the reflecting structure can be calculated and displayed.
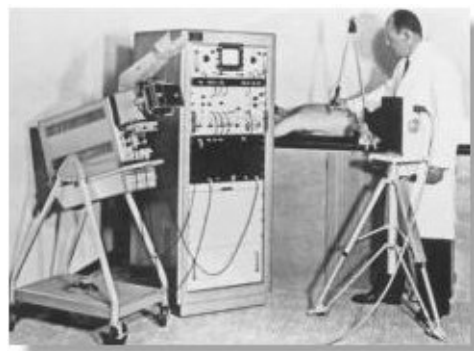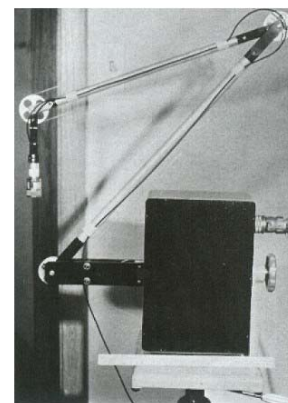
Figure 1.1 Mechanical scan ultrasound system in 1962 [www.ob-ultrasound.net].

For a single element ultrasound transducer, it is necessary to scan the probe to form a cross-section image of the area of interest. Figure 1.1 shows an early mechanical scanning ultrasound system. However, the slow scan velocity, low resolution and the discomfort of the friction on the skin prevent the further development of the mechanical

scanning. With the development of the electronics, new ultrasound transducer with

electronic scanning functions was invented. It is called phased array.
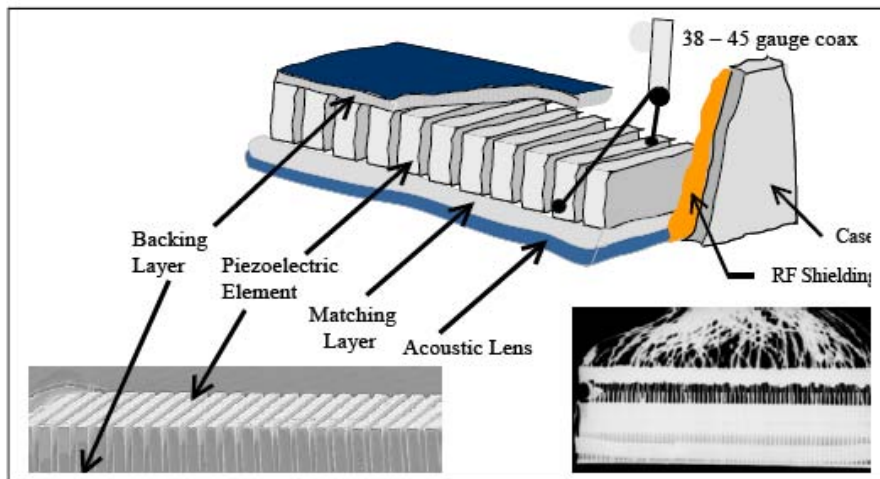
Figure 1.2 Schematic structure of a phased array transducer [www.4sonora.com].

Figure 1.2 gives an example of an ultrasound array transducer, including the

piezoelectric element arranged in a constant pitch, the matching layers which are used to

increase the transmission efficiency, the backing layer for elements support and

backward ultrasound attenuation, and the acoustic lens for the focus of ultrasound wave.

The active element, the matching layers and the backing layer are the essential parts for

an ultrasound transducer. The functionality of every part will be discussed later in

details.
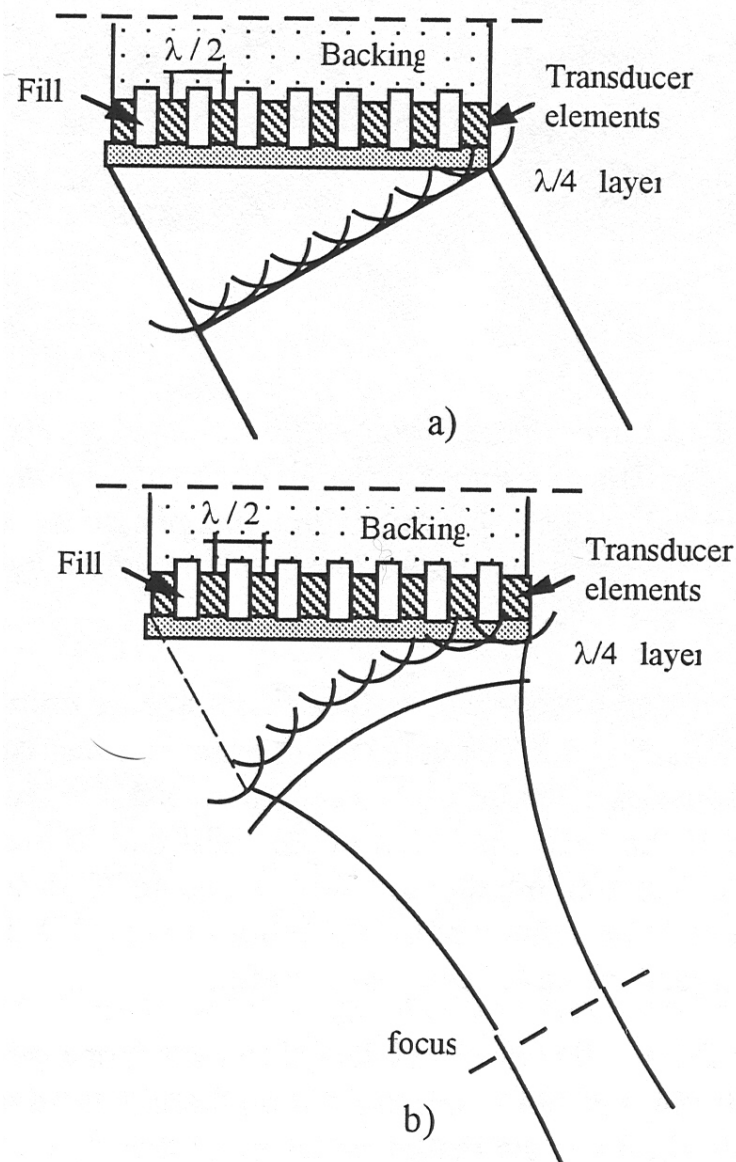
Figure 1.3 Steering the beam with phased array (a), and electric focusing (b) [Bjørn et. al, 2000].

The working principle of a phased array is schematically shown in Figure 1.3. By transmitting from left element first and then sequentially towards the right with a defined delay between each element, the beam can be steered at an angle as illustrated in the Figure1.3 (a). The direction of the beam can be found by drawing the spherical

waves emitted from each element. The interference between the element waves results

into the steered beam, according to Huygens' principle. By varying the delay for the

transmission line on each of the elements, we can steer the beam within a sector. By

introducing an additional spherical delay between the elements, we obtain electronic

steering of the focused beam as illustrated in Figure 1.3 (b). These are the two most

typical functions of phased array transducers.

There are different types of commercial ultrasound transducer products available

for different diagnostic purposes as shown in Figure 1.4. Main medical ultrasound

transducer manufactures are Philips, GE, Toshiba and etc.

Figure 1.4 Ultrasound diagnostic system and transducers available with different
functionalities [www.medical.philips.com].

1.3   Recent Development Trends and Single Crystal

Transducer

One of the recent development trends for ultrasound imaging techniques is the novel transducers which can provide 3-D image, or even 4-D (live 3-D image scanning) [Siemens, 2004]. These can only be realized with high data processing speed. Another trend is to develop ultra-high frequency transducers, such as 100 MHz above single elements [Zhang et. al, 2006] or over 30 MHz array transducers [Gottlieb et. al, 2005; Gottlieb et. al, 2006]. The ultra-high frequency transducer may provide high resolution images for medical diagnosis.

Novel matching system for the improvement of the transmission efficiency is another focus point to many researchers. Both the triple matching scheme [Edmiston et. al, 2005] and tapped matching layer [Shohei et. al, 2002; Felix et. al, 2001] have been proposed by researchers with better acoustic matching efficiency. But the complexity of these matching layers prevents them from wide use in commercial products.

Nevertheless, since the development of the lead-zirconate-titanate (PZT) ceramic, little improvement could be found for the piezoelectric materials. The piezoelectric material in an ultrasound transducer is a fundamental determinant of system image quality. Piezoelectric transducer elements are responsible for delivery of ultrasound

energy into the scanned tissue and for converting returning ultrasound echo into electric signals. Their coupling efficiency in converting electrical energy to mechanical energy or vice versa is a key factor for image quality and penetration. Despite many innovations over recent decades in signal processing and beam former architecture, the piezoelectric material, PZT or PZT composites, has been the best-in-class material used for medical imaging for almost 40 years. However, as a polycrystalline compound (ceramic), due to imperfect alignment of the individual dipoles, only 70% polarization could be achieved with corresponding constraints in the electromechanical coupling efficiency of the material. The development of the ultrasound transducer technology seems to meet the bottle-neck on the active materials [Chen et. al, 2004].

The appearance of larger piezoelectric coefficient and electromechanical coupling factor single crystals PZN-PT ($Pb(Zn_{1/3}Nb_{2/3})O_3$-$xPbTiO_3$) and PMN-PT ($Pb(Mg_{1/3}Nb_{2/3})O_3$-$xPbTiO_3$) opens a window for high performance single crystal ultrasound transducer development. Large electromechanical coupling factor and piezoelectric constant (k_{33} of 92% and d_{33} of 1500 pC/N) of <001> oriented PZN-PT single crystals were first reported by Kuwata et al. in 1982 [Kuwata et. al, 1982]. Yamashita et al. continued the research in early 1990's [Hosono et. al, 1999] on PZN-PT crystals and studied the possible applications of using the materials for medical

imaging. Park and Shrout [Park et. al, 1997] reported extremely high strain observed in

PZN-PT and PMN-PT crystals. In the past few years, these lead-based piezocrystals

have been extensively studied by many research groups and have attracted much

attention for actuators, sonar, medical imaging and other electromechanical applications

[Chen et. al, 2005].

Since 1997, the US Office of Naval Research (ONR) and Defense Advanced

Research Projects Agency (DARPA) have funded more than 60 million US dollars of

research projects in this field. Scientists have made significant progress in crystal

growth technologies, optimizing material properties and prototyping various types of

single crystal devices. The data proved that the ultrahigh electromechanical properties

(k_{33} of 93% and d_{33} of 2000-2500pC/N) could be utilized for improved sensitivity,

bandwidth, and source levels of various Navy-type devices and medical ultrasound

transducers.

Traditional PZT Ceramics
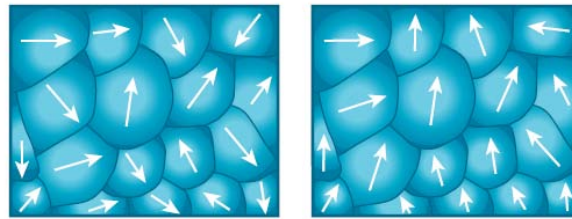
Before poling   After poling

PureWave Crystal Technology
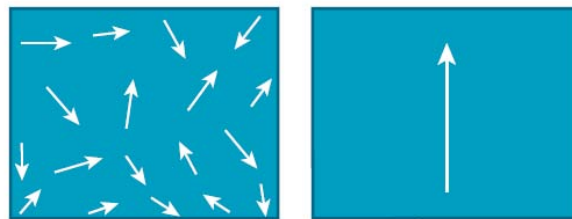
Before poling   After poling

Figure 1.5 Schematic comparison of dipole reorientation during poling of PZT and
Single Crystal [Chen et. al, 2004].

PZT ceramics must be subjected to a poling process (application of an external

electric field) to align dipoles within polycrystalline materials to create its piezoelectric

effect. In conventional PZT ceramics, due to the constraint of the grain boundaries, only

a fraction of dipoles can be aligned by an electric field and thus not all dipoles

contribute to the acoustic response of the material. In contrast, single crystal materials,

such as PMN-PT, are more uniform and exhibit fewer defects, lower losses and no grain

boundaries. When these crystals are poled at the preferred orientation, near perfect

alignment of dipoles (almost 100%) can be achieved (for simplicity, here we assuming

that the poling direction of the single crystal is long the vertical direction), as shown in

Figure 1.5 [Chen et. al, 2004]. With the help of its multi-domain configuration, PMN-PT single crystal shows dramatically enhanced electromechanical properties compared to PZT ceramics [Zhang et.al, 2001].

Table 1.1 Comparison of material properties of PZT and PMN-PT single crystal.

Properties	PZT-5A	PZT-5H	PMN-PT Single Crystal
Density (10^3 kg/m³)	7750	7500	8,000
Dielectric constant before poling at 1 kHz	1600	2800	6,000· 7,000
Dielectric constant after poling at 1 kHz	2000	3400	5,000· 6,000
Dielectric loss tan• at 1kHz(%)	2	2	<0.1
Curie temperature (•)	365	190	150
Coupling factor k_{33}	0.705	0.75	0.933
k_{33}'	0.68	0.68	0.824
k_t	0.49	0.505	0.64
Piezoelectric constant d_{33} (pC/N)	374	593	2,500
Voltage-output constant g_{33} (10^{-3} Vm/N)	24.8	19.7	43
Sound velocity v_t (m/s)	4350	4560	3,600
Acoustic impedance Z (10^6 kg/m²s)	34	34	28.8
Frequency constant Nt (Hz•m)	1890	2000	1,800· 1,900

Table 1.1 shows an example of the comparison of the properties between PZT ceramics and PMN-PT single crystal. Compared to PZT ceramics, improvements in the piezoelectric constant and electromechanical coupling factor of PMN-PT single crystal promise the high performance of the single crystal ultrasound transducers, such as broad bandwidth and high sensitivity.

1.4 Literature Review in Single Crystal Transducer Development

Several companies including Toshiba, Philips, Tetrad, Humanscan, Penn State

University/TRS Technologies, Vermon, and etc. have been studying single crystal medical ultrasound transducers. Toshiba was the pioneer in this field, started working on single crystal development and phased array transducers for medical imaging applications in the 1990's [Chen et. al, 2005].

Saitoh and Yamashita et al. [Saitoh et. al, 1999] reported a 3.7MHz phased array transducer using PZN-9%PT crystal in 1999. By modifying the standard process, a 128-channel phased array probe having less than 10% inactive elements was fabricated to realize improved sensitivity and broader bandwidth for echocardiography. The echo amplitude of the PZN-9%PT single-crystal probe is about 5 dB higher than that of the conventional PZT ceramic probe, and the fractional bandwidth is about 25% broader. The quality of B mode images of the PZN-9%PT probe satisfies those of the two conventional PZT ceramic probes whose frequencies are 2.5 and 3.75 MHz, respectively. The Doppler sensitivity of the PZN-9%PT probe is about 5 dB higher than that of the 3.75 MHz PZT probe. The remarkable improvement of this PZN-9%PT probe has been confirmed, but the improvement of probe fabrication process still needs to be studied in the next phase.

Oakley and Zipparo from Tetrad [Oakley et. al, 2000] worked on a 1-3 PZN-PT single crystal composite transducer and a PMN-PT transducer in 2000. First of all,

single crystals have been developed with coupling factors for length resonators as high

as 0.95. Array elements with high sensitivity and bandwidths of over 120% have been

modeled. Single element composite transducers with single crystal of PMN-PT ranging

from 100% bandwidth with 7 dB insertion loss to 140% bandwidth with 18 dB insertion

loss have been demonstrated. This is far better than what has ever been achieved with

PZT ceramics.

Single crystal relaxor ferroelectrics of PZN-8%PT were investigated by Ritter et al

[Ritter et. al, 2000] for potential application in ultrasound transducers in 2000.

Ultra-high length extensional coupling (k_{33}) of 0.94 was observed, a 25% increase over

Navy Type VI PZT ceramics. The thickness extensional coupling (k_t) of 0.48 was

comparable to PZT compositions, and the compliance S^E_{33} was a factor of six greater.

To maximize height extensional coupling (k'_{33}), while minimizing length extensional

coupling k_{31} in array elements, it was necessary to align the elements along the <100>

crystallographic direction in the x-y plane. Mode coupling plots and test samples for

array elements determined that width-to-height ratios of less than 0.5 were desired,

similar to the requirement for polycrystalline PZT ceramics. Modeling of 1-3

composites and experimental results demonstrated that thickness coupling greater than

0.80 could be achieved with a 40% to 70% volume fraction of PZN-PT. Although this is

a substantial increase over PZT 1-3 composites, with a thickness coupling coefficient of 0.66, it represents a smaller fraction of the length extensional coupling k_{33}. This reduction may be a consequence of the increased compliance of PZN-PT, which results in significant clamping by the polymer matrix. Ultrasound transducers fabricated using PZN-8%PT 1-3 composites achieved experimental bandwidth up to 141%.

In 2002 Rhim et al at Humanscan [Rhim et. al, 2002] developed a 2.6 MHz phased array transducer with PMN-PT. Adequate size and quality of PMN-PT single crystal for use in the medical ultrasound probe were obtained by Bridgman method. Their work proved that the piezoelectric, electromechanical, and elastic properties of PMN-PT single crystals in rhombohedral phase were larger than those of PMN-PT in tetragonal phase. The electromechanical coupling factors k_{33} and k_{33}' of (001) oriented PMN-PT were larger than those of commercial PZT polycrystalline ceramics, and piezoelectric constant d_{33} was a factor of two greater than that of PZT ceramics. The echo amplitude of the PMN-PT single crystal probe is about 6 dB higher than that of the commercial PZT probe, and the -6 dB bandwidth is about 30 % broader. The capacitance at 1 kHz of PMN-PT single crystal of each element is about 60% larger than that of commercial PZT probe. The harmonic mode image quality of PMN-PT probe is superior to commercial PZT probe and color Doppler sensitivity of PMN-PT probe is about 5 dB

higher than that of PZT probe.

Michau et al from Vermon   [Michau et. al, 2002] reported a 64 element transducer in 2002. The specific nature of single crystal, as compared to standard piezoceramics, requires the development of new transducer micro-machining and manufacturing processes to enhance the sensitivity and bandwidth of the transducers. The dicing speed of 0.6 mm/s was proved to be the adequate linear speed to avoid cracking and chipping within the crystals. The achieved phased array is a 5 MHz configuration with a circular aperture within 10 mm diameter and 2 mm height. Final results show the improvement achieved with single crystals by comparing these results to those obtained on standard piezoceramic phased array with an increase of 14% in bandwidth and 3.4 dB in sensitivity.

Hackenberger et al published similar data in 2003 [Hackenberger et. al, 2003], with even wider bandwidth for a single element Doppler transducer built with 1-3 PMN-PT composite. In fact, initial measurements after fabrication indicated rather poor response. Exposure to pressure during lapping and molding and/or high temperature when the backing layer was cast and cured may have caused partial depoling. After repoling, the transducer resulted in much improved properties with a 120% bandwidth at 5.2 MHz central frequency. The transducer can operate from sub harmonic of 1.75MHz to 2nd

harmonic of 7.0MHz.

In 2005, Lu and Proulx from Seimens Medical Solutions [Lu et. al, 2005] reported a 90% bandwidth PMN-PT transducer fabricated with the same matching and tuning inductor of a commercial PZT product, which has only 77% bandwidth. Nevertheless, the bandwidth of the single crystal probe was not as wide as predicted (102%). Typically the measured spectrum rolls off sooner at high frequency. One speculation is that the "soft" single crystal may be clamped by the kerf filler, bond epoxy, or matching layers. The clamping effect, of which the 1-D model does not take into consideration, may compromise the high frequency performance. Another theory is that the crystal microstructure may be damaged during processing, and the wavelength at high frequency is more relevant to the damaged structure. Comparison between a 2.5 MHz PMN-PT phased array and a 2.5 MHz triple matching PZT array indicated that single crystal transducers with very high electrical impedance may not match multi-layer PZT array performance for low frequency applications. Because of processing challenges with the thin crystal layer and the potential for depoling or fatigue during long term usage, it is also not likely that single crystals can be used above a center frequency of 6 MHz. So the preferred application of single crystals appears to be for low to mid-frequency (3-5 MHz) arrays, preferably with relatively large elements.

Philips started its single crystal transducer investigation in 1997. The first low frequency phased array transducer has already been released to customers in Nov. 2004 in IE 33 system shown in Figure 1.6. So far, the single crystal ultrasound transducer has received excellent market acceptance [Chen et. al, 2004]. The commercialization of the PMN-PT transducer has already clearly depicted the future of the application of single crystal technology in the medical diagnostic field.

Figure 1.6 IE 33 ultrasound system based on single crystal technology from Philips [www.medical.philips.com].

1.5   Motivation of Thesis Work

Even though a lot of research work on PMN-PT single crystal phased array transducers has been done, only Philips has available product in the market. This is due to the reason that a number of challenges need to be overcome before a marketable product can be released. The main challenges and issues are:

1. Due to low fracture toughness, PMN-PT single crystal suffers from easy crack propagation during processing such as lapping and dicing which leads to a low yield. By reducing the crystal internal stress, developing or optimizing the lapping and dicing techniques, mass production of single crystal phased array transducer is possible. Technically, there are a lot of rooms for developing or improving the fabrication process such as dicing speed, dicing depth, and matching/backing materials etc.

2. PMN-PT has a relatively low Curie temperature (about 120˚C), and practically, the piezoelectric property starts to decrease significantly at a temperature of 80˚C. Therefore, the wire welding and epoxy curing process must be precisely controlled at temperatures below 80˚C in order to avoid depolarization and

degradation of piezoelectric properties. Low temperature process therefore needs to be developed.

3. Since PMN-PT possesses different acoustic impedance (about 29 MRayls) compared to PZT (34 MRayls), the conventional backing and matching materials used for PZT are not suitable for PMN-PT. Preliminary results from other researchers showed that with those backing and matching layers suitable for PZT, the PMN-PT single crystal transducer does not show much advantages over PZT transducer. Therefore, novel matching scheme, new types of backing and matching materials for broad bandwidth PMN-PT transducers should be developed.

This thesis work focuses on developing process, and study physics behind, in fabricating large bandwidth PMN-PT single crystal phased array ultrasound transducer for medical imaging application. With the help of computer simulation (using PiezoCAD based on KLM model), we are going to narrow down the selection of suitable backing and matching materials. The success of this project may help mainland China in developing high performance and high value-add medical imaging product, and obtain deep understanding in single crystal ultrasound transducer design, fabrication and characterizations.

1.6   Outline of Thesis

In Chapter 2, the fabrication process of ultrasound transducer is introduced, including the preparation and characterization of the matching, backing and the PMN-PT single crystal. Phased array transducers' fabrication flow was then depicted step by step, followed by the characterization method of the array transducers.

Simulation study of the PMN-PT ultrasound transducer will be discussed in Chapter 3. Acoustic design optimization methods will be introduced in detail from backing layer selection, matching layer's thickness and effective acoustic impedance optimization and the PMN-PT single crystal coupling factor improvement, etc.

Two prototype phased array transducers using PMN-PT single crystal with different design schemes were fabricated and characterized. The characterization results of these two prototype transducers are reported in Chapter 4.

Chapter 5 is the conclusion of the thesis and perspective view of future work.

CHARPTER 2

TRANSDUCER FABRICATION AND CHARACTERIZATION INTRODUCTION

Fabrication of ultrasound transducer array is a challenging work. In particular, the acoustic properties of backing and matching materials, including their acoustic impedance, sound velocity and attenuation, are very important for the performance of transducer. For example, in order to obtain a decent performance, the thickness of each matching layer and active layer should be well controlled in fabrication process. In addition, the electrical connection from the electrode on the PMN-PT single crystal to signal or ground line should also be well designed to avoid unwanted vibration. This chapter describes the techniques and materials implemented in the fabrication of phased array transducers and the characterization method of the transducers such as the pulse-echo measurement.

2.1 General Introduction to Fabrication Flow
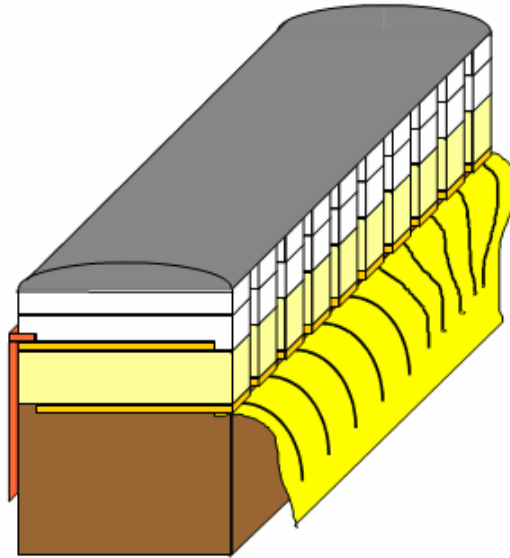
Figure 2.1 The schematic structure of an ultrasound array transducer.

Figure 2.1 is a schematic structure of a phased array transducer. To fabricate a phased array transducer, sequence of the fabrication flow should be carefully considered. Figure 2.2 shows the conventional fabrication flow steps.

The phased array transducer fabrication starts from the surface treatment of the crystal, followed by electrode coating, acoustic layer stacking, array fabrication and kerf filling steps. For our prototype, we put our effort on the performance of the transducer with different acoustic design (matching and backing), so we may pass over the housing steps and acoustic lens stacking to make the process simpler.
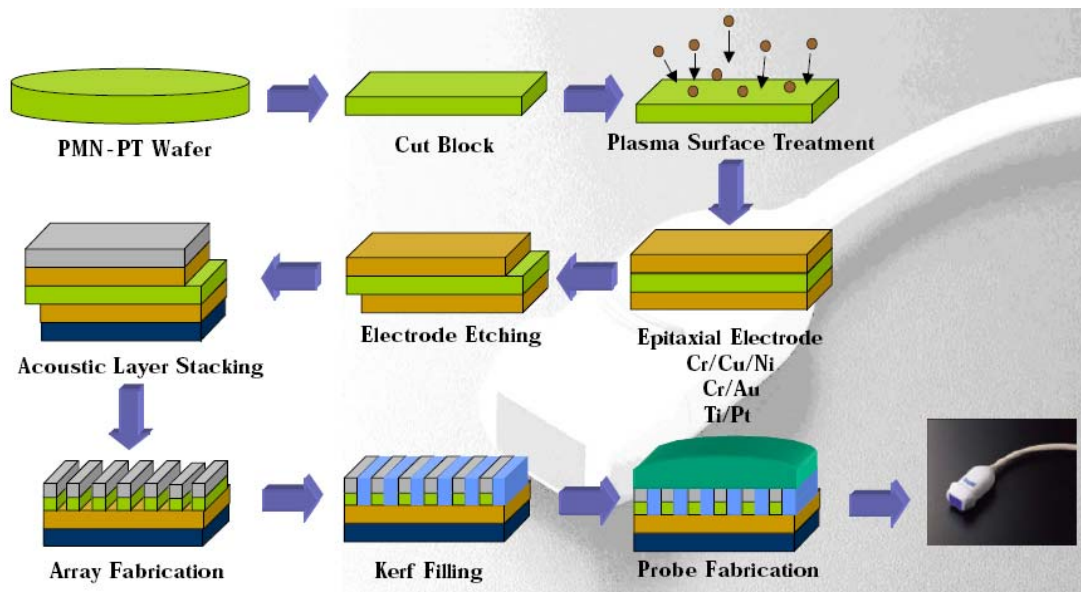
Figure 2.2 Fabrication flow of a phased array transducer based on PMN-PT single crystal.

2.2 Introduction of the Electrode and Electric Connection

Electrode in the ultrasound transducer provides the electric field needed for the active elements. High-quality electrode is essential for the performance of the ultrasound transducer. Sputtered Au/Cr electrode is widely used in commercial products. The thickness of the sputtered Au/Cr electrode is only several hundreds of nanometer, which is invisible for the ultrasound frequency wave. So Au electrode is a good choice for the high frequency transducers. Gold is a soft metal with good flexibility which could sustain the thermal expansion. It is also an inert material which does not interact with most chemicals. This helps to keep the sample surface clean from the oxidation in air and other contamination introduced in the fabrication processes. With the Cr

adhesion layer, the connection between the Au electrode and the active material may be greatly improved.

The solid electric connections from electrode to signal and ground wires are critical for ultrasound transducers working in a vibration status. Solder welding method is the widely used method for solid connection in conventional transducer fabrication. But for the low Tc material PMN-PT which begins to depole at $60℃$, the solder welding method may not be suitable. The solder should be heated up to above $100℃$ to be melted and attached onto the electrode. Even with the help of fan pointed to the sample surface, the thermal conductive electrode will still transmit most of the heat from the solder to the sample and cause the PMN-PT depoling. The low temperature curing conductive epoxy is a good candidate in such kind of requirement.

2.3   Introduction of Matching Layer for the Transducer

2.3.1   Acoustic Matching in Ultrasound Transducer

To solve the problem of acoustic impedance (Z) mismatch, matching layer was invented in ultrasound transducer structure. The matching layer is a thin layer with designed acoustic impedance and thickness lying between the active element and the

front load of the ultrasound transducer to improve the transmission efficiency of the

ultrasound on the interface.

Acoustic impedance (Z) is the quantity analogous to the momentum in ultrasound.

In classical mechanics, momentum is equal to the product of mass and velocity;

whereas in ultrasound, density (ρ) replaces the mass and is then multiplied by the

velocity of sound (C) in the medium. The definition of acoustic impedance Z is giving

by [Hedrick et. al, 1995]:

$$Z = \rho C . \tag{2.1}$$

Similar to electrical resistance which is the degree of difficulty experienced by

electrons when traversing through a specific type of material, this quantity Z is a

measure of the resistance of sound when passing through a medium.   Table 2.1 shows

the sound Velocities, mass densities, compressibility, and acoustic impedances of some

biological and non-biological materials.

Table 2.1 Acoustic parameters for typical isotropic, homogeneous, elastic materials
[Angelsen, 2002].

Material	Mass density kg/m^3	Compressibility 10^{-12}m^2/Nt	Sound velocity m/s	Acoustic impedance MRayls
Biological material:				
Fat	950	508	1440	1.37
Neurons	1030	410	1540	1.59
Blood	1025	396	1570	1.61
Kidney	1040	396	1557	1.62
Liver	1060	375-394	1547-1585	1.64-1.68
Spleen	1060	380-389	1556-1575	1.65-1.67
Muscles	1070	353-393	1542-1626	1.65-1.74
Bone	1380-1810	25-100	2700-4100	3.75-7.4
Non biological material:				
Air (0℃)	1.2	$8*10^{-6}$	330	0.0004
Rubber	950	438	1550	1.472
Fresh Water (25℃)	988	452	1497	1.48
Salt Water	1025	416	1531	1.569
Polystyrene	1120	143	2500	2.8
Hard PVC	1350	175	2060	2.78
Typ. Araldit	1200	160	2300	2.8
Silicon, RTV-11	1260	739	1000	1.26
Quartz	2650	11.4	5750	15.2
PZT-5A	7750	5.65	4350	33.71
Gold	19290	4.93	3240	62.5
Aluminum	2875	9	6260	18

It is apparent that different materials have different acoustic impedances. As we know, for a typical ultrasound transducer, the acoustic impedance of the front load (body tissue) is about 1.5 MRayls; while for the active material, for example PMN-PT single crystal, its acoustic impedance is as high as 30 MRayls. Due to their different acoustic impedances, (see Figure 2.3), without a matching layer lied between the body tissue and the PMN-PT single crystal, most of the vibration energy exited from the active element will be reflected back into the active material at the transducer/body interface. This is called acoustic impedance mismatch.

Interface

PMN-PT Single Crystal
30 MRayls

Body Tissue
1.5 MRayls
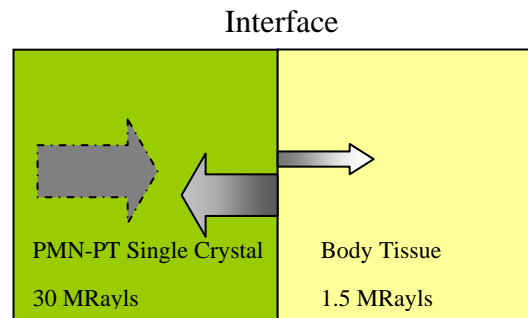
Figure 2.3 Schematic diagram showing the acoustic mismatch at the transducer/tissue interface.

The reflection coefficient α_R and transmission coefficient α_T, which define the energy proportion being reflected/ transmitted at the interface of two different acoustic media (Z_1 and Z_2), can be calculated with the flowing equations:

$$\alpha_R = \left(\frac{Z_2 - Z_1}{Z_2 + Z_1} \right)^2 , \qquad (2.2)$$

$$\alpha_T = \frac{4 Z_1 Z_2}{\left(Z_1 + Z_2 \right)^2} . \qquad (2.3)$$

It has been calculated in the reported work [Edmiston et. al, 2005] that with a single intermediate layer (matching layer), the transmission coefficient could rise from 18% to 34%. As shown in Figure 2.4, increasing the number of the matching layer between front load and the active element increases the transmission efficiency further. It is apparent that more matching layers may improve performance of the ultrasound transducer by increasing the transmission efficiency. However, the complexity and cost will also increase with the number of matching layers. In commercial products, double matching layer design is the most popular acoustic design, which provides well transmission efficiency and also acceptable cost and fabrication complexity.
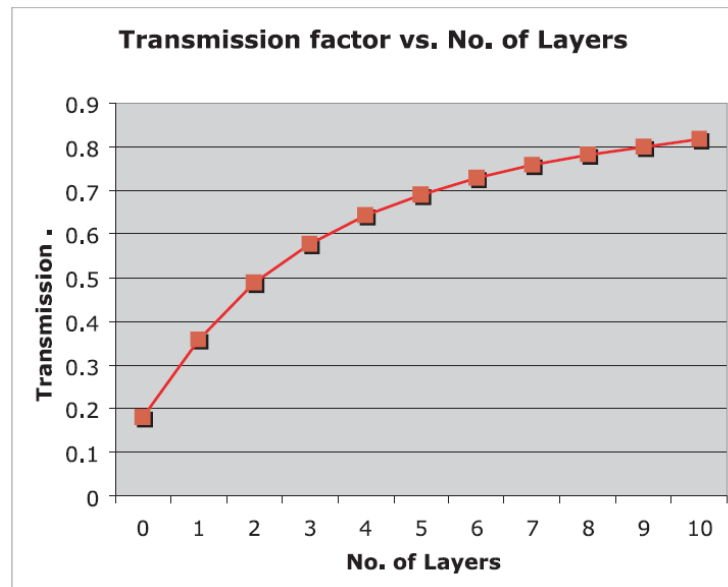
Figure 2.4 Transmission efficiency as a function of number of matching layers
[Edmiston et. al, 2005].

2.3.2   Matching Layer Theory Introduction

A_1

Backing	Active	Matching	Load
Z_B	Element	Layer	Z_L
	Z_0	Z_1	
	t_0	t_1	

A_2

Backing	Active	First	Second	Load
Z_B	Element	Matching	Matching	Z_L
	Z_0	Layer	Layer	
	t_0	Z_1	Z_2	
		t_1	t_2	
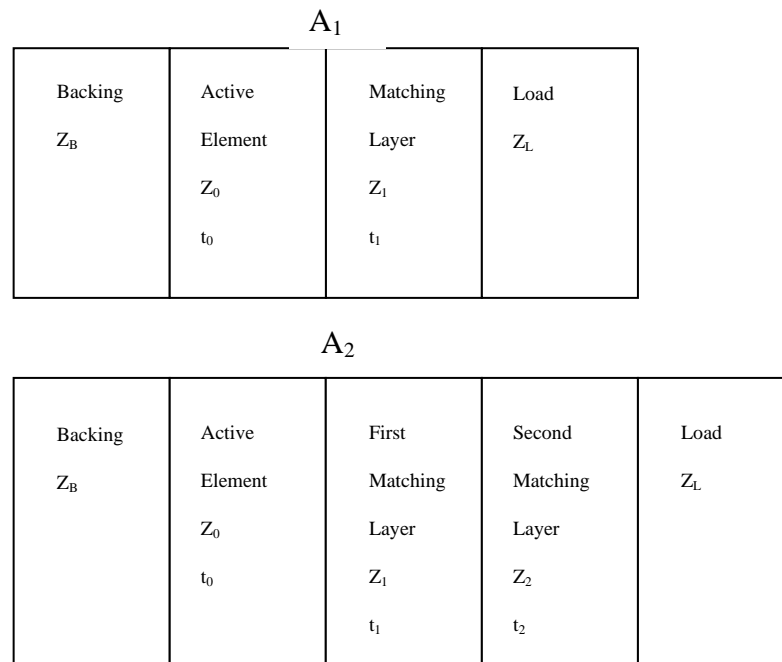
Figure 2.5 Model of ultrasound transducer with one or double-layered matching.

One of the well-accepted theories of acoustic matching is the transmission line theory. According to this theory, given the physical model of ultrasound transducers with one matching layer shown in Figure 2.5, the input impedance at the interface A_1 is given by:

$$Z_{A1} = Z_1 \frac{Z_L \cos k_1 \delta_1 + jZ_1 \sin k_1 \delta_1}{Z_1 \cos k_1 \delta_1 + jZ_L \sin k_1 \delta_1} , \tag{2.4}$$

where k_1 is the circular wave number, and δ_1 is the thickness of the matching layer.

For the center frequency of the transducer, when the thickness of the matching layer δ_1, and the acoustic impedance Z_1 are:

$$\delta_1 = (2m+1)\frac{\lambda_1}{4} , \tag{2.5}$$

$$Z_1 = \sqrt{Z_0 Z_L} , \tag{2.6}$$

we can get $Z_{A1}=Z_0$ from the above equation (2.4). The impedance matching is realized with the proper designed matching layer.

In the double matching layer model, if we choose

$$\delta_1 = (2m+1)\frac{\lambda_1}{4}, \tag{2.7}$$

$$\delta_2 = (2m+1)\frac{\lambda_2}{4}, \tag{2.8}$$

$$Z_1 = \sqrt[4]{Z_0^3 Z_L} , \tag{2.9}$$

$$Z_2 = \sqrt[4]{Z_0 Z_L^3} , \tag{2.10}$$

the input impedance on the interface A_2 will be $Z_{A2}=Z_0$, and acoustic impedance

matching in the double matching system will be obtained.

There are other theoretical models describing the acoustic matching in ultrasound transducers, for example Mason Model and KLM model etc. Table 2.2 lists examples of the results of the requirement of the acoustic impedance of the matching layers from these models.

Table 2.2 Matching layers' impedances from different models for a PZT transducer [Fen et. al, 2001].

Theoretical model	Z_0	Single matching	Double matching		Triple matching			Z_L
		Z_1	Z_1	Z_2	Z_1	Z_2	Z_3	
Traditional Model	35	7.2	15.9	3.3				1.5
Mason Model		4.3	9.1	2.4	22.3	7.7	2.9	
KLM Model		4.5	8.5	2.4	14.2	4.1	1.9	

Theoretically, the thickness of the matching layer should be exactly quarter wavelength from the equations mentioned formerly. In real fabrication, considering the frequency shift when the front matching layers are attached onto the transducer, the thickness of the matching should be multiplied by a factor. In single matching layer case, this factor is 1.16, and for double matching, it should be 1.18 from former experience [Fen et. al, 2001].

2.3.3   Criteria of Matching Layers

The acoustic matching theory suggests that for acoustic matching, the thickness of

the matching layer should be a quarter of its wavelength when the transducer is working

on its central frequency. For example, a 3 MHz central frequency transducer requires

the thickness of the matching layer to be about 200 μm if the sound velocity of the

matching layer is 2400 m/s. Therefore, it can be seen that sound velocity is an important

factor in the fabrication parameter considerations. The higher the sound velocity, the

thicker the matching layer. High sound velocity in matching material can bring

advantages to the transducer's matching layer fabrication, especially for high frequency

transducers where the matching layer is very thin.

For an ultrasound transducer, the function of the matching layer is to transmit the

sound vibration into the load, so the sound attenuation in the matching material should

be as low as possible to avoid the energy loss in the matching layer. Attenuation

includes the effects of both scattering and absorption which are manifested by the

amplitude reduction as the ultrasound wave propagates through a medium. This can be

described as follows:

$$A = A_0 \exp(-az), \tag{2.11}$$

where A and A_0 represent the amplitudes of the sound after and before the attenuation,

and z is the distance sound travels through. The attenuation coefficient a is given by the sum of the scattering coefficient α_s and the absorption coefficient α .

Scattering is a very important interaction between ultrasound and tissue. It is a kind of nonspecular reflection, which is responsible for providing the internal texture of organs in the image. The scattering occurs because the interfaces are small, less than several wavelengths. Each interface acts as a new separate sound source, and sound is reflected in all directions. Scattering by small particles in which the linear dimensions are smaller than the wavelength is called Rayleigh scattering. These nonspecular reflections have a strong frequency dependence (f^2 to f^6), which may make them useful in characterizing tissue.

Absorption is the only process where sound energy is dissipated in a medium. All other modes of interactions (reflection, refraction, scattering and divergence) decrease the ultrasonic beam intensity by redirecting the energy of the beam. Absorption is the process where ultrasonic energy is transformed into other energy forms, primarily heat. The absorption of an ultrasonic beam is related to the beam's frequency and to the relaxation time and viscosity of the medium. The relaxation time describes the rate at which molecules return to their original positions after being displaced by a force. If a substance has a long relaxation time, the molecules may be moved back toward their

original positions as the wave crest (compression) strikes them. More energy is required

to stop and then reverse the direction of the moving molecules, and this produces more

heat (absorption). The ability of molecules to move past one another determines the

viscosity of a medium. For instance, a low-viscosity fluid flows more freely than a

viscous one. Since frictional forces must be overcome by vibrating molecules, and thus

more heat is produced in the high-viscosity fluid.

In conclusion, for a matching material, low attenuation property, low scattering,

short relaxation time and low viscosity should be the desired properties.

2.3.4   Matching Materials
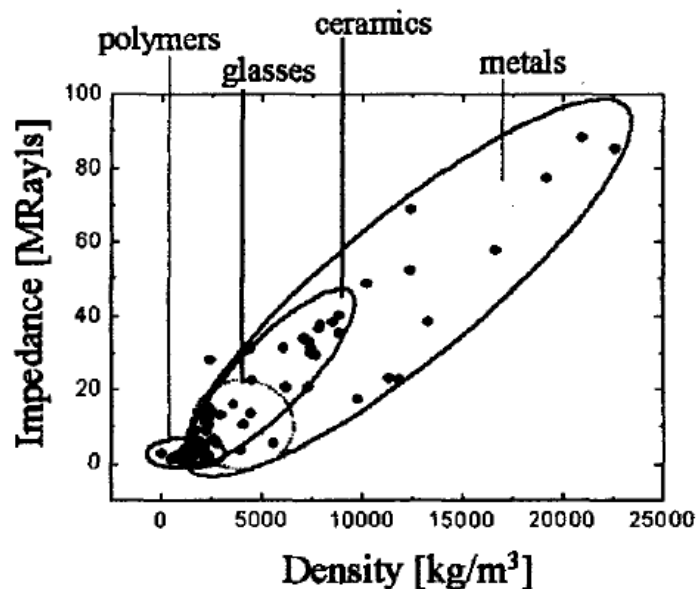
Figure 2.6 Acoustic impedance of polymers, glass, ceramics and metals as a function of
bulk density [Rhee et. al, 2001].
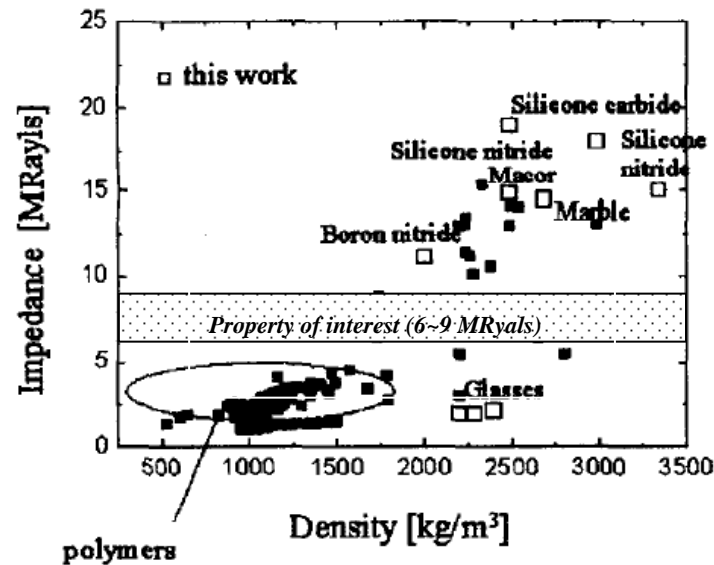
Figure 2.7 Acoustic impedances of materials with densities up to 3500 kg/m^3
[Rhee et. al, 2001].

The impedances of various materials, including polymers, ceramics, glass and metals are shown in Figure 2.6. It is apparent that there is a correlation between the acoustic impedance Z and the bulk densities. It can also be seen that there are very few monolithic material in the range of 6~9 MRayls (see Figure 2.7) which are suitable for the first matching layer of a double layer matching scheme for PMN-PT single crystal. Therefore incorporating composites to fabricate matching layers is a good choice.

To make composite matching layer, epoxy is the most popular matrix material for its convenience in mixing and curing processes. Epoxy also shows stable properties after curing. There are several requirements for a desired epoxy:

1. Low viscosity to enhance the mixing with the powder to eliminate the air bubbles in
    the mixture;

2. Low curing temperature in order to cast matching or backing directly on to active
    materials;

3. High glass transition temperature;

4. Hard after curing, which makes it easy for mechanical process such as dicing,
    polishing, with small or no deformation after machining;

5. Low heat transmission property, to protect the heat generated from the active
    element to the patients' body.

For a composite acoustic matching material, the components must appear homogeneous in the interested frequency range. Therefore, the microstructure scale of the individual component should be in the order of $< \lambda/10$ to make it invisible for the ultrasound. Otherwise, deleterious effects such as excessive attenuation may arise.

In order to decrease the attenuation of the matching materials, there are several other requirements for additive selection. First, even smaller particle size is preferred to eliminate the scattering phenomena on the matrix/particle interface. Second, low density additive material is preferred to decrease the relaxing time of the additive particle in the

composite (when the vibration transmit through the composite, the different inertia of

additive particle and the matrix will cause the different relaxing time of their vibration.

More different inertia, more relative vibration happens between the additive particle and

the matrix, and then more heat will be generated by this kind of attenuation).
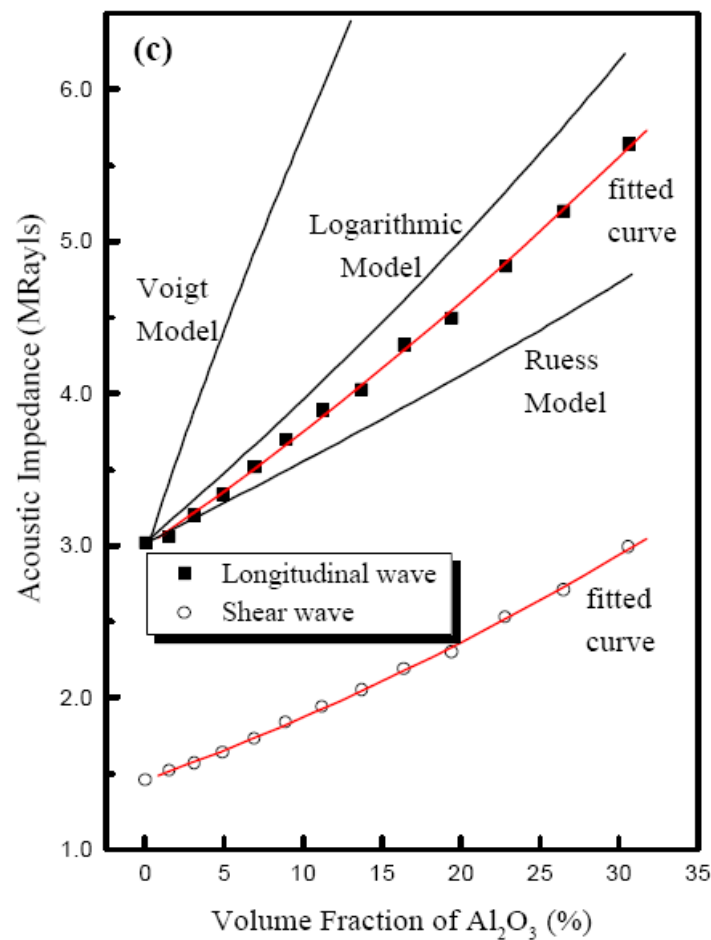
Figure 2.8 Variation of acoustic impedance with the volume fraction of alumina in
EPO-TEK 301 [Wang et. al, 1999].

As shown in Figure 2.8, higher volume fraction of additive (alumina) in composite

results in higher acoustic impedance. Voigt model, logarithmic model and Reuss model

have been used to fit the acoustic property of Alumina/ Epoxy composite. Simulation

results based on these models are also show in this figure for comparison [Wang et. al,

1999]. From the curve above, we could adjust the volume fraction of the additive to

prepare the composite with desired acoustic impedance for matching materials.

2.4   Introduction on Backing Material for the Transducer

2.4.1   Acoustic Mechanism for Backing

Backing is a very important part for ultrasound transducers, especially for array

transducers, which serves as the rigid supporting substrate for the array elements.

Figure 2.9 shows the performance of ultrasound transducers with no backing (air),

light backing and heavy backing respectively. The air backing transducer shows high

sensitivity, but the ring-down last for a long time. In the frequency spectrum it means a

narrow bandwidth of the transducer. With the increase of the backing's acoustic

impedance, sensitivity of the transducer decreases, but the ring-down time becomes

shorter, and thus the bandwidth in frequency spectrum increases dramatically.
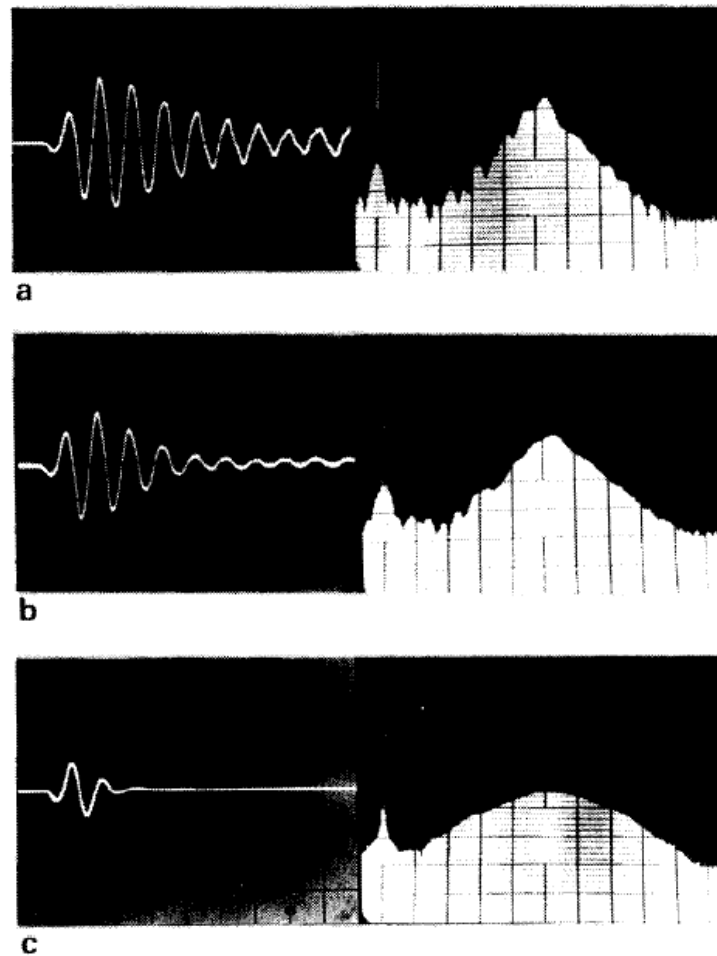
Figure 2.9 Echo pulse shape and frequency spectra obtained in an experimental echo system using transducers with backing only: (a)—air backing, Z_B=0; (b)—light backing, Z_B=5 MRayls; and (c)—heavy backing, Z_B=24 MRayls [Persson et. al, 1985].

We know that when an AC electric field is applied on the electrode of the active element of an ultrasound transducer, the vibration will be generated on both surfaces of the element. On the front surface, the vibration will be transmitted by the matching system to the body tissue for medical diagnostics. While on the back surface of the active element, the same acoustic mismatch as mentioned in the matching will happen

also. With no backing (air backing), for the dramatic mismatching between piezoelectric

materials (around 30 MRayls) and air (about 0 MRayls), almost all the energy directed

to the back of the active element will be reflected back into the active element and cause

the active element vibrating for a long time, i.e., long ring-down waveform shown in

Figure 2.7(a). With a heavy backing, there will be a small acoustic impedance mismatch

at the element/backing interface, and therefore, the effect of the reflected signal on the

active element's ring-down process will be small.

For an ultrasound transducer, bandwidth is the most important parameter. Broader

bandwidth means higher axial resolution, higher sensitivity in a broad frequency range,

and more functions for different diagnostic targets. The low sensitivity of a transducer

could still be improved by the following electrical processing steps. Most of the

ultrasound transducers choose a proper backing to improve the transducers' bandwidth

performance. For nondestructive testing transducer which requires high axial resolution,

heavy backing (close to the driving materials) is used on sacrificing the transducer's

sensitivity. While for medical ultrasound transducer, the mismatch between the

transducer active materials and the body tissue already makes the transmission

efficiency very low, and the small different acoustic impedance (reflection or scattering)

between different body tissues makes the ultrasound imaging more difficult for clearly

depicting the structure of the tissue. So light backing (around 5 MRayls) is chosen for medical ultrasound transducer to get a balance of the transducer bandwidth and sensitivity.

Since the vibration reflected from the backing direction of the active element is unwanted, the vibration energy reflected on the end of backing surface to the active material should be well controlled to achieve good performance. The well accepted standard of the attenuation in the backing layer is about -100 dB. For the sound wave travels from the top surface to the bottom and reflected on the backing/air interface and travels again through the backing to the top surface, the attenuation in the backing thickness should be -50 dB. The attenuation is proportional to the thickness of the materials the sound traveling in. So if we have a high attenuation backing material, the thickness of the backing could be small as shown in the equation:

$$\alpha x = -50 dB, \tag{2.12}$$

where α is the attenuation coefficient, and x is the thickness of the backing.

To fabricate a compact transducer is always the target of manufacturers. With a small volume, not only the portability of the ultrasound imaging system can be achieved, the possibility of intrusive type ultrasound transducer which could be placed near the target of interest by inserting into the human body may also be realized. This kind of

ultrasound transducer could overcome the high attenuation effect of the ultrasound

brought by the body tissue. The high attenuation or high absorbing property is preferred

for backing materials.

2.4.2   Backing Material Selection

We met the same problem when we choose the materials for matching which

should have acoustic impedance around 8 Mrayls. For backing materials, we need light

(around 5 MRayls) or heavy (around 10 MRayls) acoustic impedance materials which

could hardly be found in monolithic materials. Composite is the proper choice of the

backing material again.   Epoxy/metal powder mixture is chosen for its convenience in

mixing and acoustic property control as we mentioned in the matching part.

In addition to the requirements similar to matching epoxy, good heat transmission

property allowing the transmission of the heat generated by the active element to the

back of the transducer is needed. This can reduce the temperature rising of the

transducer and help to keep the active materials working in a good status.

For a composite backing, in terms of acoustics, the composite being comprised of

two or more materials must appear homogeneous in the frequency range of interest. So

the microstructure scale of the individual components should be in the order of $<$ 1/5 of

the smallest dimension of the transducer elements [Baumgartner et. al, 2005].

In order to increase the attenuation property of the backing materials, several requirements should be met for the additive selection. First, comparably bigger particle size is required to increase the scattering function of the particle, of course in the safe scale of the acoustic homogeneous composite. Second, high density additive material is preferred to increase the relaxing time of the additive particle in the composite and thus improve the attenuation property. Third, absorbing material is needed to increase the attenuation function, such as hollow glass sphere, silicone bead and etc. These kinds of soft materials could transfer the compressing stress in the sound traveling process to shear stress because of their low rigidity (easy to deform under stress). The amplitude of the vibration in the sound transmission direction could be dramatically decreased by this kind of stress redirection.

As shown in the Figure 2.10, high volume fraction of additive (tungsten) in the composite gives high acoustic impedance. Voigt model, logarithmic model and Reuss model have been used to predict the property of this kind of 0-3 composite [Wang et. al, 1999]. Simulation results based on these models are also shown in the figure for comparison with experimental results. From the curve above, we could adjust the volume fraction of the additive to increase the composite acoustic impedance to the desired light or heavy acoustic impedance.
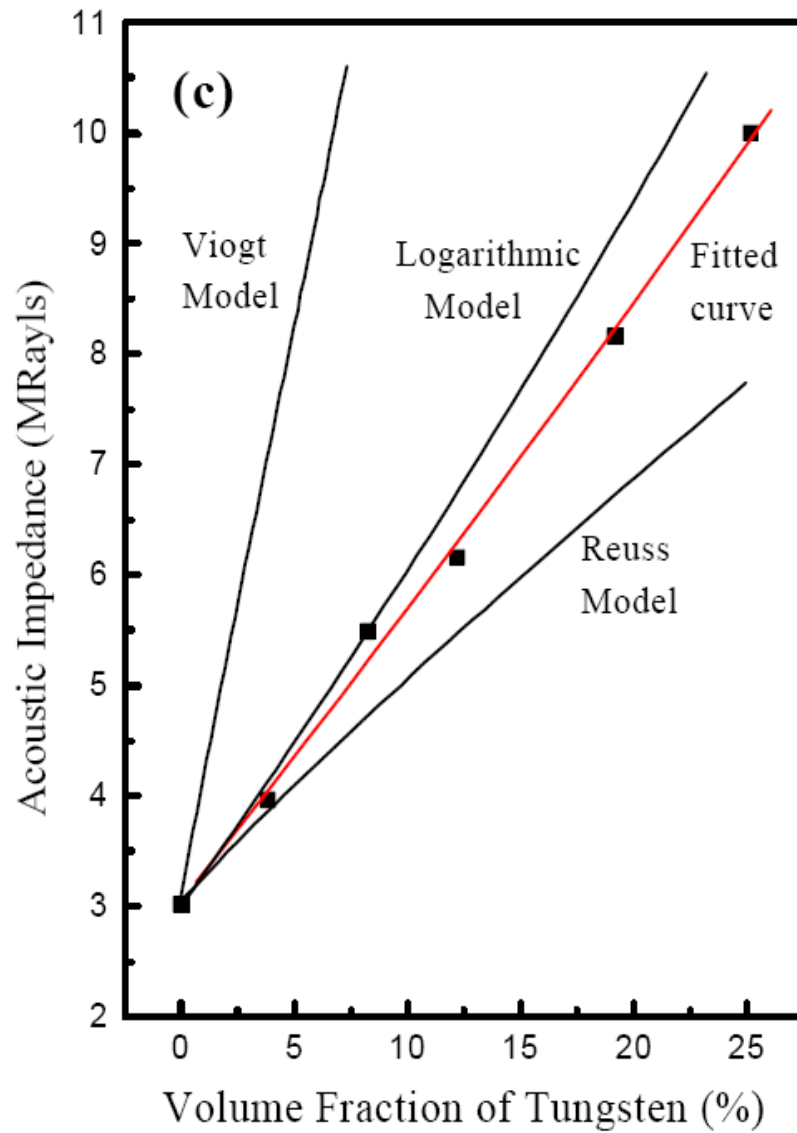
Figure 2.10 Variation of acoustic impedance with the volume fraction of tungsten in
EPO-TEK 301 [Wang et. al, 1999].

2.5   Introduction of Element Dicing

Element dicing is the last step for transducer fabrication (not including the filling

and housing steps). In this step, a blade is used to cut into the double matching layer, the

PMN-PT single crystal and the backing to form separated elements in the design pitch

to make an array transducer in which all the elements work on their own signal source.
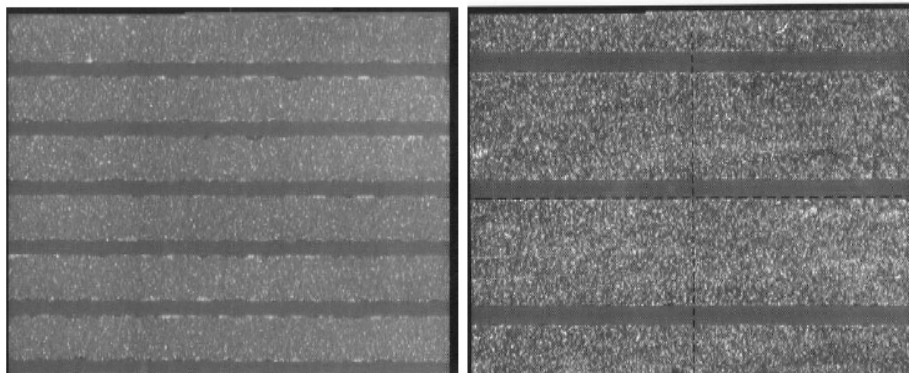
Figure 2.11 Diced PMN-PT samples with different linear speeds (0.8 mm/s above and
0.6 mm/s below) [Michau et. al, 2002].

The machining process of the single crystal is critical to the transducer

performance, especially the dicing process which might introduce defects such as crack

or depoling. Because of the nature of single crystals, specific provisions for crystal

micro-machining are required to avoid cracks and chipping within the crystals. Some

dicing experiments are needed to be conducted to define the most suitable dicing

parameters (processes set up, linear and wheel speeds) for the single crystals.

Systematic investigation of this parameter from 0.2mm/s to 1mm/s leads to the selection of 0.6mm/s as adequate feeding speed. Improvements in the dicing could be seen from Figure 2.11 with two different dicing configurations. No chipping is observed in the second one with lower linear speed.

2.6   Introduction on Characterization Methods

2.6.1   Sound Velocity Measurement

Sound travels in the materials according to the vibration transmission from one particle to another. This transmission keeps as a constant speed in certain temperature, and will not be effected by the frequency of the sound traveling in the material. This gives us the advantage in measuring the sound velocity traveling in all the materials of interest with one frequency, i.e., the central frequency f_c of a transducer. On the other hand, since sound velocity changes with the material temperature, a constant circumstance temperature is needed in this measurement.
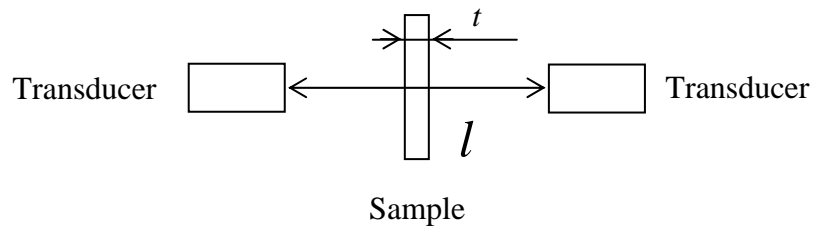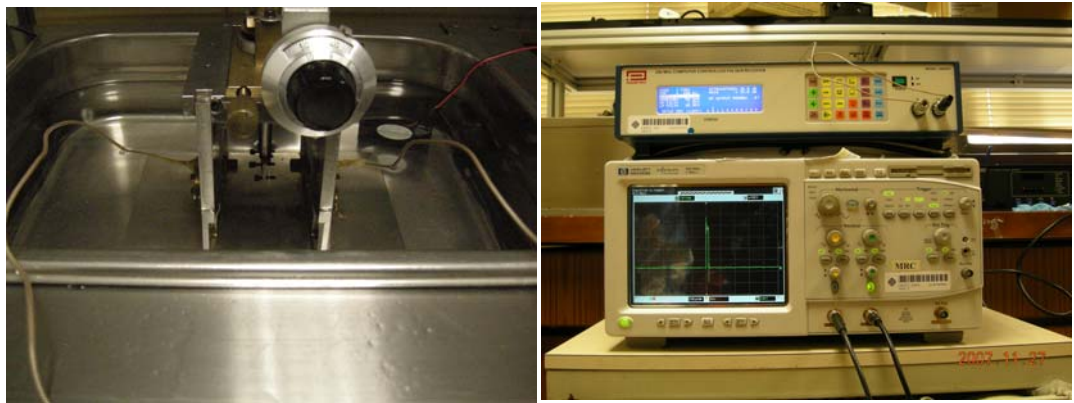
Figure 2.12 Setup for sound velocity measurement.

Figure 2.12 is a setup for sound velocity measurement. The ultrasound analyzer (Panametrics, Model 5900PR) generates a pulse from the left transducer with 10 MHz central frequency. Besides the part reflected on both silicone oil/ sample interfaces, sound wave will travel through the distance of silicone oil/ sample/ silicone oil, and be detected by the transducer on the right. Signal will be processed by the ultrasound analyzer and shown on the screen of the oscilloscope. The time of the pulse generated from the transducer on the left, and the time pulse be received by the transducer on the right, can be measured. Sound velocity in the sample at this temperature can be calculated as follows:

$$\Delta t_{oil} - \Delta t_{sample} = t(\frac{1}{v_{oil}} - \frac{1}{v_{sample}}) \,. \qquad (2.13)$$

Where l is the distance between the two transducers, which is set as 13.4 mm; Δt_{oil} and Δt_{sample} are the time needed for the sound wave to transmit through the distance l in oil without and with sample in it, respectively; t is the thickness of the sample. In this measurement, the diameter of the sample (a circular plate) should be at least double the diameter of the ultrasound transducer used which is 1 cm in the measurement. This requirement is to eliminate the shear wave effect to the sound velocity measurement.

2.6.2 Density Measurement

For irregular shape samples, the density measurement can be done by Archimedes drainage method. The dry weight of the sample (W_d) should be measured first.   The wet weight (W_w) means the weight measured when the sample is immerged in the water (ρ_w), which is given by the dry weight subtracted by the weight of the same volume of water as the sample measured. The density of the sample could be calculated as follow:

$$\rho = \frac{\rho_w W_d}{W_d - W_w} \,. \qquad (2.14)$$

When measuring the wet weight W_w, we should take care of the small bubbles attached on the sample surface which will decrease the sample's wet weight. Or, we may use volatile liquid such as ethanol to avoid the generation of the air bubble attached.

2.6.3　　Attenuation Measurement

The attenuation of the ultrasound signals is proportional to the thickness of the

homogenous material where the sound travels in. We measured the amplitude of signal

V_1 at the sample thickness of t_1, then lapped this sample down to thickness t_2, and

measured the amplitude of signal V_2. The amplitude of the signal is related to two

factors. One is the transmission efficiency determined by the acoustic impedance

mismatch of sample and silicone oil. The other is the attenuation in sample. While the

acoustic mismatch status did not change because of the same sample/silicone oil

interfaces (the sample is assumed to be homogenous with different thickness). Then it is

the thickness of the sample which affected the signal amplitude via attenuation. The

attenuation coefficient can be calculated as follow:

$$\alpha = \frac{-20\log\left(\frac{V_2}{V_1}\right)}{t_2 - t_1}. \tag{2.15}$$

When $t_1=0$, we could use the acoustic impedance measured before to calculate the

transmit efficiency α_T, then the attenuation coefficient can be calculated as:

$$\alpha = \frac{-20\log\left(\frac{\alpha_T V_2}{V_1}\right)}{t_2}. \tag{2.16}$$

2.6.4   Transducer Performance Evaluation Method

Pulse echo response is the most common test performed on single element and array transducers. This measurement provides the array element's center frequency, bandwidth and relative sensitivity which are the three most important parameters for ultrasound transducers. The setup used for pulse echo response measurement is shown below in Figure 2.13.
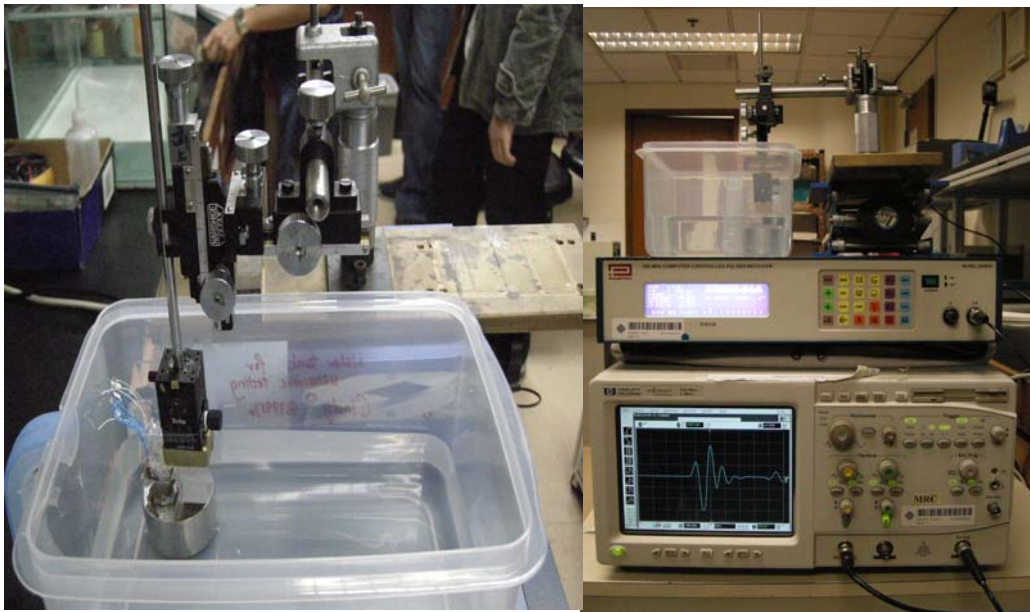
Figure 2.13 Pulse echo response measurement setup.

The transducer was characterized in a sound absorption water tank at room temperature. A polished stainless steel or quartz flat plate is placed at the post focal point of the transducer, normal to the transducer maximum response axis to reflect the ultrasound pulse back to the transducer. A standard pulse/receiver was used to excite

and receive electric signal to and from the transducer element.   Figure 2.14 gives an

example of the ring-down waveform measured in the pulse echo response. The Fourier

transform of this received time-domain echo response is depicted in Figure 2.15.
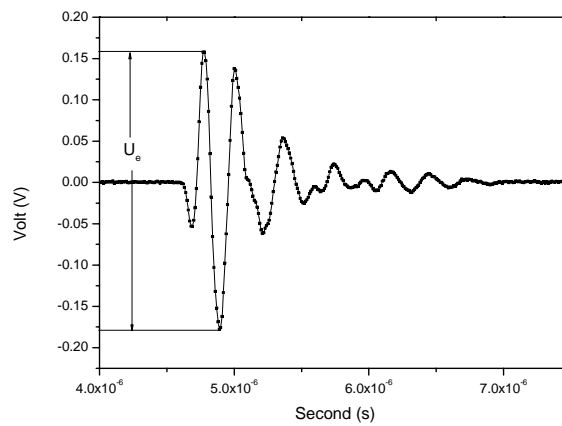
Figure 2.14 Pulse echo response of a phased array element.
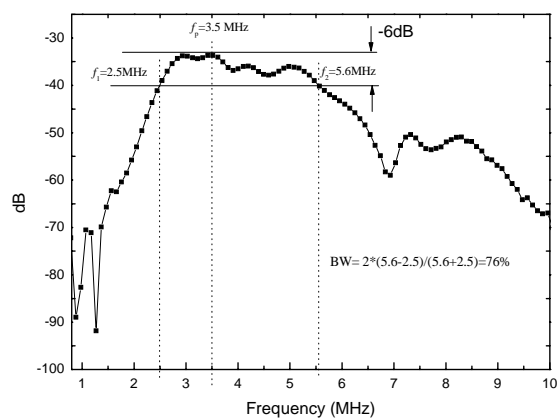
Figure 2.15 Frequency spectrum of a phased array element.

The relative sensitivity of the transducer is given by:

$$S = 20 \lg \left(\frac{U_e}{U_T} \right),$$ (2.17)

where U_e is the peak to peak amplitude of the echo waveform, and U_T is peak to peak

amplitude of the excitation pulse amplitude applied on the transducer.

The two -6 dB points of this power spectrum defined the upper and lower band

edges of the signal, f_1 and f_2 respectively. The central frequency f_c of this phased array

element is given by:

$$f_c = \frac{f_1 + f_2}{2},$$ (2.18)

and the bandwidth of this phased array element is given by:

$$BW = \frac{f_2 - f_1}{f_c}.$$ (2.19)

CHARPTER 3

MODELING OF

ULTRASOUND TRANSDUCER

There are a number of simulation tools available to aid the design of piezoelectric based ultrasound transducers. An accurate mathematical model can predict the performance of the transducer with different parameters, and thus help to decrease transducer's development time, and to reach a realistic compromise between the design and fabrication. The most widely used software for the ultrasound transducer simulation is PiezoCAD based on the one-dimensional equivalent circuit model. PiezoCAD is very useful for the selection of acoustic matching and backing layers, as well as electrical impedance matching, and therefore is always used as the first order approximation to ultrasound transducer performance.

PiezoCAD is a software for modeling the performance of single element transducer or an individual array element. It approximates the transducer elements as

one-dimensional vibrators and represents them as an equivalent electrical circuit which is called KLM (Krimholz, Leedom, and Matthaei) equivalent circuit [Krimholz et al., 1970]. There are also some other equivalent circuits such as Mason model [Mason, 1942], and the Redwood model [Redwood, 1961]. These models have been proven to be very effective in predicting the performance of single element and piezoelectric composite transducers [Ritter et al. 2000], but are limited in usefulness when modeling array elements [Cannata et. al, 2003]. As one-dimensional model, PiezoCAD can not take some factors into account for array transducers such as element crosstalk resulting from shear waves in the kerf filler, Lamb waves within the matching layers and the surface waves in the backing layers. Nevertheless, circuit analogous modes can be very useful in determining the ideal thickness and composition of matching, backing and piezoelectric layers used in array construction, as well as the impact of electrodes and epoxy bond lines on the time domain response and etc.

3.1   KLM Model
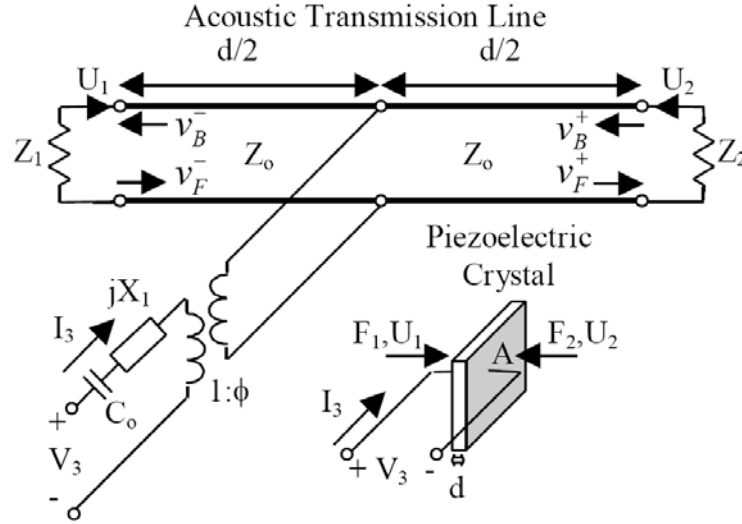
Figure 3.1 KLM model scheme [www.brl.uiuc.edu].

The KLM model used in PiezoCAD is shown in Figure 3.1. In this model, V_3 and

I_3 are the respective voltage and current applied to the piezoelectric crystal, which

produce the resulting acoustic forces F and particle velocities U at the respective faces

of the crystal. The particle velocities inside the crystal are denoted by $V_{F,B}^{\pm}$, where F

subscript indicates forward traveling waves propagating towards interface 2, the B

subscript indicates backward-traveling waves propagating towards interface 1, and the

± denote waves in the right and left half of the crystal, respectively. The model

parameters include the thickness of the crystal d, the area of the crystal A, and the

characteristic impedance Z_0 of the acoustic transmission line modeling the piezoelectric

crystal. Z_1 and Z_2 are the respective radiation impedances of the medium into which the

crystal is radiating. In order to complete the model, it is also necessary to include a capacitor C_0, impedance jX_1, and a transformer with the ratio $(1: \varphi)$ that converts the electrical signal into the appropriate acoustical values. C_0 results from the resonator consisting of a dielectric, the piezoelectric crystal, between two excited conducting surfaces. The values for these parameters as given by Krimholtz et al. in 1970 are:

$$Z_0 = \rho cA, \tag{3.1}$$

$$C_0 = \frac{\varepsilon A}{d}, \tag{3.2}$$

$$X_1 = \frac{h^2}{\omega^2 Z_0}\sin\left(\frac{\omega \cdot d}{c}\right), \tag{3.3}$$

$$\phi = \frac{\omega Z_0}{2h}\cos ec\left(\frac{\omega \cdot d}{2c}\right). \tag{3.4}$$

Where ε is the permittivity of the piezoelectric without applied voltage, h is the piezoelectric pressure constant for the crystal, ρ is the density, and c is the speed of longitudinal sound waves in the crystal.

3.2   Simulation Parameters and Results
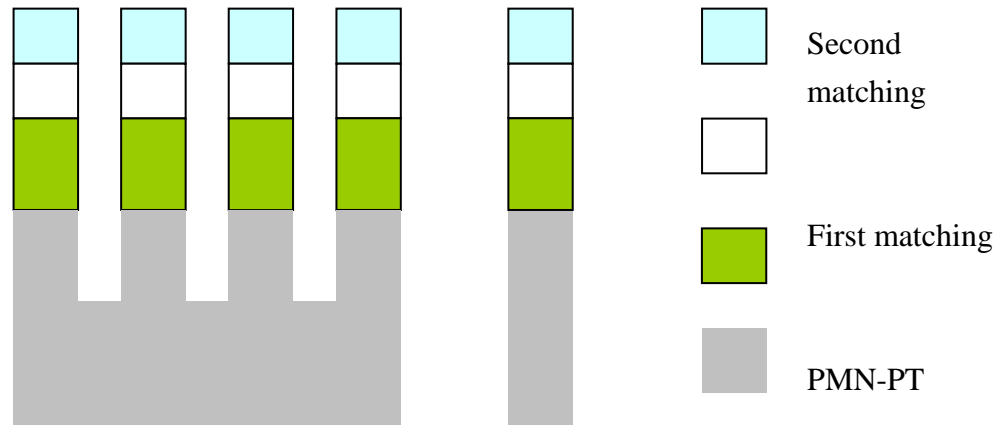
Figure 3.2 The basic geometry of a 4-element prototype array (on the left) and the
one-dimension model used in the PiezoCAD simulation (on the right).

The KLM model based software package PiezoCAD (Sonic Concepts,
Woodinville, WA) was selected for the evaluation of the designed transducer, and the
initial prototype design is depicted in the above Figure3.2. Table 3.1 lists the design
parameters of the transducer.

Table 3.1 Design parameters of phased array transducer.

Transducer type	Phased array
Active material	PMN-PT single crystal
Center frequency	3.2 MHz
Front load	Body tissue (water)

3.2.1 Active Element Parameters

Element Width

To simulate and predict the performance of the PMN-PT phased array, parameters such as the dimension of the active element and the electromechanical coupling factor need to be input. Phased array is superior for its functions of electric steering and focusing. To be able to steer the beam at an angle, the individual element needs to radiate energy as much as possible in the forward direction. To realize this, the width of the elements must be less than one wavelength. Also, in order to avoid grating lobes in directions other than the desired beam, the distance between the centers of neighboring two elements must be less than $\lambda/2$ of the wavelength. Therefore to get an adequate aperture of the transducer, a large number of elements, typically 64 to 128 elements, are necessary in making the width of the transducer in the range of 32 to 64λ. For a 3 MHz transducer, if we chose 96 elements, the aperture is 48λ, which is about 26 mm.
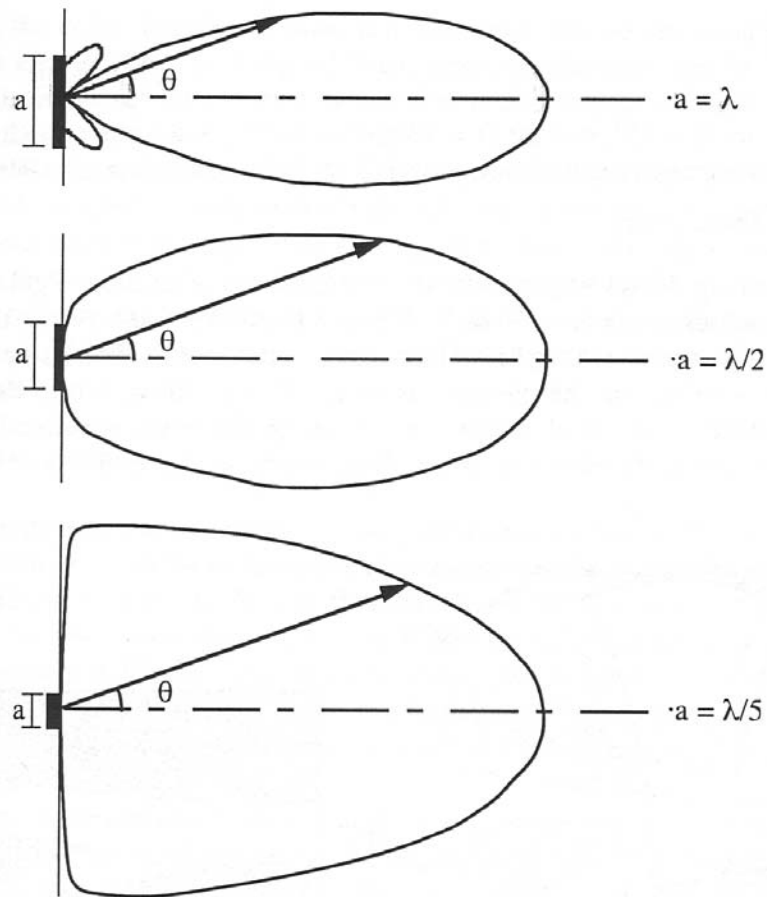
Figure 3.3 Beam profiles for CW excitation of elements with different widths.

The beam profile for elements with width λ, $\lambda/2$, and $\lambda/5$ are shown in Figure 3.3. We can see that, for a phased array, to have adequate energy at an angle of $45°$, the width of each element should be $\lambda/2$ or less.

In real fabrication, element width is defined as the result of the element pitch subtracted by the kerf width introduced by the dicing step. From the above introduction of the phased array working principle, we know that the element pitch of the array

element should be about λ/2. For the 3.2 MHz center frequency transducer, it is 260 μm. If the kerf width introduced in our dicing step is around 80 μm, the width of the transducer element is thus 180 μm.

Element Thickness

Single-element transducers always work at their resonate frequencies, and the thickness of the active element is designed to be about λ/2 at its center frequency to realize the transducer's resonation. Frequency constant N_t depicts the relation of the element thickness t and the transducer resonant frequency f_r as follows:

$$N_t = f_r \times t .$$ (3.5)

For array transducer, the center frequency design is a little bit complicated compared to the single element transducers. A known phenomenon is that the position and shape of the f_r resonance depends significantly on the length and width dimensions of the ceramic slab, as well as the thickness. There is a strong influence due to model coupling of the other dimensions on f_r. But for the anti-resonant peak, f_a, it is very well defined and repeatable. This is due to the reason that the anti-resonance (or parallel resonance) frequency is fundamentally related only to the ceramic thickness, and not influenced by model coupling. Also, as the amount of poling is increased in a given material, f_a will remain nearly constant; while f_r will steadily decrease until the material

is completely poled. Thus, f_a depends on the velocity and thickness; while f_r depends on

the motional reactance, which varies with the poling state of the material and

cross-coupling to other vibration modes. Due to these reasons, a more predictable way

to specify and construct ultrasound transducers is to specify ceramic dimensions, and

matching layer thickness, referred to f_a, rather than f_r. Starting with a ceramic that

resonates at f_a, a broad-band transducer design usually has a nominal center frequency

much lower than f_a. This is because of several downshifting factors, which will be

explained below. The final center frequency of an ultrasonic array transducer may be

expressed as [McKeighen et. al, 1998]:

$$f_c = Ds * f_a = d_{s1} * d_{s2} * d_{s3} * d_{s4} * f_a, \qquad (3.6)$$

where f_c is the transducer design center frequency, f_a is bulk ceramic anti-resonant

frequency, Ds is the total downshift factor. The down shift factor Ds is the product of a

series of down shift factors.

1. d_{s1} is downshift factor #1, which is introduced by the lower frequency resonance

   caused by dicing ceramic into sub-elements, i.e. the acoustic velocity is lower

   because of side wall boundary conditions (wave guide); d_{s1} is 0.82 (when kerfs are

   later filled with polymer resin);

2. d_{s2} is downshift factor #2, which is introduced by the mass loading effect of acoustic stack (matching layers and backing) on ceramic resonance; d_{s2} is about 0.95;

3. d_{s3} is downshift factor #3, which is introduced due to frequency dependent attenuation of RTV lens or face material; d_{s3} is about 0.93;

4. d_{s4} is downshift factor #4, which is due to the fact that pulser circuits usually have very low impedance (5 to 10 ohms). Thus, energy is more easily coupled to the low impedance resonance peak f_r, rather than the higher impedance resonance f_a; d_{s4} is about 0.78.

The total transducer frequency downshift factor can be [McKeighen et. al, 1998]

$$D_S = d_{s1}*d_{s2}*d_{s3}*d_{s4} = 0.56, \tag{3.7}$$

and $f_c = 0.56 * f_a$. Therefore, to start a transducer design (linear or phased array), one wants to order ceramic with bulk resonance f_a in the slab of frequency approximately 1.77 times the nominal transducer design center frequency. For example, for a 3.2 MHz linear array, one would order ceramic with $f_a = 5.7$ MHz. For PMN-PT single crystal we choose 0.33 mm slab which could meet the requirement.

Element Length

For single element transducer design, there is a very important consideration for the active element dimensions, the element area. For commercial product, the input impedance of the transducer element is set to be 50 Ω in order to match the electrical circuit impedance. The input impedance of the transducer element is defined by the active element area and its dielectric constant. Tuning of the active element area is always used to adjust the input impedance of an ultrasound transducer.

For array transducers, in order to realize the linear or phased array function, the area of every single element is always too small (the width of the element is about λ or even smaller). The consequence of the small array element is its large electrical impedance (100-600 Ω) which dose not fit the 50 Ω requirement. So electrical tuning is usually used to match the electrical impedance of the transducer element to 50 Ω, and the element length is no longer considered in electrical impedance design. On the other hand, other requirements in transducer design should be considered when setting the element length, for example, power, focus on the elevation direction, and transducer house, etc. In our designed prototype, we chose 13 mm element length which is the same as a commercial product we are developing. Excluding the room for electrical

connection of the signal and ground wire, the exact element length is set to be 11.4 mm

in our simulation.

Electromechanical Coupling Factor

Electromechanical coupling factor defines the ability of the piezoelectric material

to convert the electric energy to mechanical energy (vibration) or vice versa. It is an

important factor determining the performance of the ultrasound transducer which works

on the energy transformation between electrical status and vibration status.

Measurement of this parameter is done by means of impedance analyzer. The equation

used to calculate the electromechanical coupling factor k_t is as follows:

$$k_t^2 = \frac{\pi f_r}{2 f_a} \tan\left(\frac{\pi(f_a - f_r)}{2 f_a} \right),$$

(3.8)

where f_r and f_a are the resonate and anti-resonate frequencies, respectively. Parameters

of the PMN-PT single crystal element used in the simulation are listed in the table blow:

Table 3.2 Parameters of the PMN-PT element used in simulation.

Active elements thickness	0.33 mm
Element width	0.18 mm
Element lenght	11.4 mm
k_t	61 %

3.2.2   Optimization of Backing and Matching

Backing Acoustic Impedance

We firstly attempt to predict the transducer performance by adjusting the backing material's property – acoustic impedance. Backing materials with different acoustic impedances ranging from 3 to 13 MRayls have been used in the transducer's simulation. Figure 3.4 shows the simulated bandwidth and sensitivity of the performance of the transducer as a function of backing material's impedance. In this simulation, PMN-PT single crystal is used as the active element material, and the acoustic impedances of the double matching layers are 6.31/2.15 MRayls respectively. One can see that transducer's bandwidth rises from 30% to as high as 67%, almost double the original value, showing great improvement while using heavy backing to substitute the light backing. The decrease of the transducer's sensitivity from -42 dB to -49 dB can also be seen when the acoustic impedance of the backing changes from 3 to 13 MRyals in simulation results. Nevertheless, compared to the big improvement of the transducer's bandwidth, a -7 dB sensitivity sacrifice is acceptable.
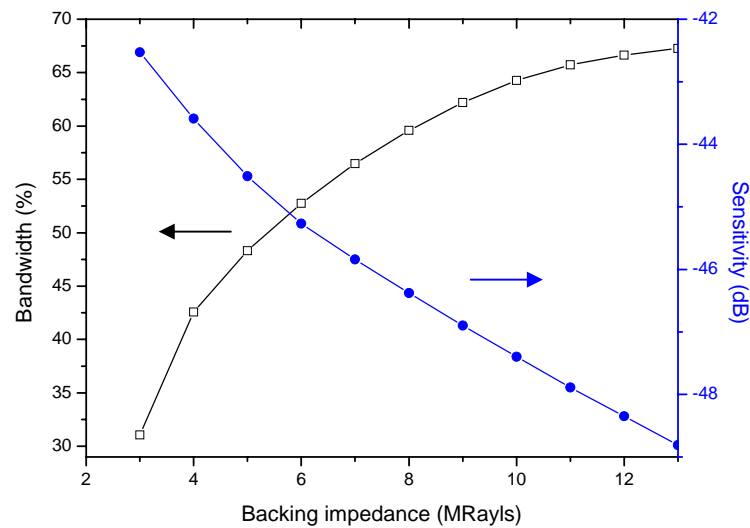
Figure 3.4 Simulated transducer's bandwidth and sensitivity with different backing acoustic impedances with 6.31/2.15 MRyals double matching.

It is apparent from the simulation result that the effect of the backing's acoustic impedance is significant to the transducer's bandwidth. On one hand, with heavy backing, more energy may be transmitted and absorbed by the backing material and decrease the ring down time, thus the bandwidth of the ultrasound transducer will be increased. On the other hand, more vibration energy absorbed by the backing layer, means less energy for detection; i.e. the sensitivity of the transducer will decrease.

Matching Layer Acoustic Impedance

The matching layers work for the acoustic matching between active element and the body tissue. According to the KLM model, their acoustic impedance should meet the specific requirement to serve for the matching function. The calculation of the

matching layers' acoustic impedance is determined by the front load (body tissue) and the active materials.

A lot of methods have been made to optimize the acoustic design of the matching layer's acoustic impedance, including the one based on experience or computer simulation aid optimization. Here a so-called effective acoustic impedance method is introduced. The formulas for matching layers derived always assume an air load on the back side of the transducer ceramic. But it will be more flexible in optimizing the design trade-off if the impact of the back side loading and impedance on the ceramic are included in choosing the matching layer impedance values applied to the front side of the transducer.

We usually assume that the acoustic impedance of a PZT ceramic is about 33 MRayls in calculating the required matching layer impedances as discussed in KLM model. However in the effective acoustic impedance approach, we use the KLM model or other transmission line models to calculate the average acoustic impedance as a function of frequency first, looking into the face of the ceramic. This value will be influenced by the load on the back side of the ceramic and by the electrical tuning, because of the electrical-acoustic coupling. Then, we calculate the average effective impedance of the face of the ceramic over the bandwidth of interest, say 70 %, and use

this value to plug into the transmission line equations to calculate the desired quarter

wave matching layer values. In this example with 3.0 Mrayls backing, over a 70 %

bandwidth, the effective average acoustic impedance of 33 Mrayls PZT is only 18.5

Mrayls, the resultant matching layer values would be:

First matching layer: $Z_1 = Z_c^{4/7} Z_L^{3/7} = 6.31$ MRyals.

Second matching layer: $Z_2 = Z_c^{1/7} Z_L^{6/7} = 2.15$ MRayls.

The experiment results proved the simulation results of the effective acoustic

impedance method, by giving a transducer bandwidth of about 72% using the matching

layers calculated above. From this example, we can find that the PZT ceramic whose

acoustic impedance are always recognized as 33 MRayls, still works well if we define

its acoustic impedance as only 18 MRayls in the matching layer design, much lower

than the well accepted ones. That means the effective acoustic impedance of the active

material is more important in matching layer design than the conventional measured

acoustic impedance which is the product of material density and sound velocity.

Viewing the the effective acoustic impedance, McKeighen [McKeighen et. al, 1998]

used 70% bandwidth in designing to calculate the effective acoustic impedance in the

frequency range of interest. But how should we do if we want to improve the bandwidth

performance without knowing the desired bandwidth? The method above does not fit

our requirement anymore. However with the help of PiezoCAD, we can solve this problem easily. If we define the effective acoustic impedance of the PMN-PT single crystal as the input parameter, and calculate the matching layer's acoustic impedance using the same KLM model, and define the transducer bandwidth with different matching systems as output parameters. Once the transducer bandwidth reaches the peak on bandwidth axis, the effective acoustic impedance parameters used in the matching acoustic impedance calculation on effective acoustic impedance axis should be the one we want to find with specific backing material. Table 3.3 lists the matching layer's acoustic impedance calculated with different PMN-PT effective impedances. The Figure 3.5 below shows the simulation results.

Table 3.3 Matching layers' acoustic impedance calculated with different PMN-PT effective impedances.

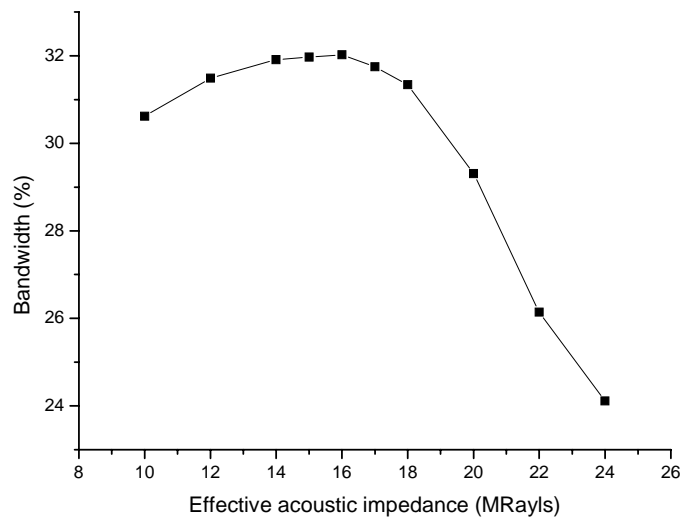| PMN-PT Effective impedance	First matching impedance	Second matching impedance
Z_{eff}	$Z_1 = Z_{eff}^{4/7} Z_L^{3/7}$	$Z_2 = Z_{eff}^{1/7} Z_L^{6/7}$
24	7.31	2.23
22	6.96	2.20
20	6.59	2.17
18.54	6.31	2.15
18	6.21	2.14
17	6.01	2.12
16	5.80	2.10
15	5.59	2.08
14	5.38	2.06
12	4.92	2.20
10	4.44	1.97

Figure 3.5 Simulated transducer's bandwidth with different matching layer's impedances on the same 3 MRayls light backing.

From the above curve, we can find that the peak emerges at 17 MRayls of active

element's effective acoustic impedance. Therefore, 17 MRayls can be recognized as the

effective acoustic impedance of the PMN-PT single crystal working with a 3.0 MRayls

backing. The acoustic impedance of PMN-PT is not 29 MRayls any more in this

circumstance. This effective acoustic impedance may be used in the matching layers

design, which results in the acoustic impedance of the first and second matching of 6.0

and 2.1 MRayls, respectively. Matching material at this range is much easy to prepare

compared to the high-acoustic impedance matching layers. According to the simulated

results, the bandwidth improvement brought by the tuning of the effective acoustic of

the active element is from 24% to 32% with the same 3 MRayls backing.

Matching Layers Thickness

As called quarter-wave matching, the thickness of the matching layer is always

recognized as quarter wavelength at the transducer's center frequency. However as a

conclusion from experimental results, in reality, it is set to be 1.18 times of the quarter

wavelength of the center frequency [Fen et. al, 2001]. Actually, the center frequency

shifts in the transducer fabrication with different parameters including backing,

matching and etc. So the optimization of the thickness of the quarter matching layer is

necessary when considering the center frequency shift phenomenon in transducer design.
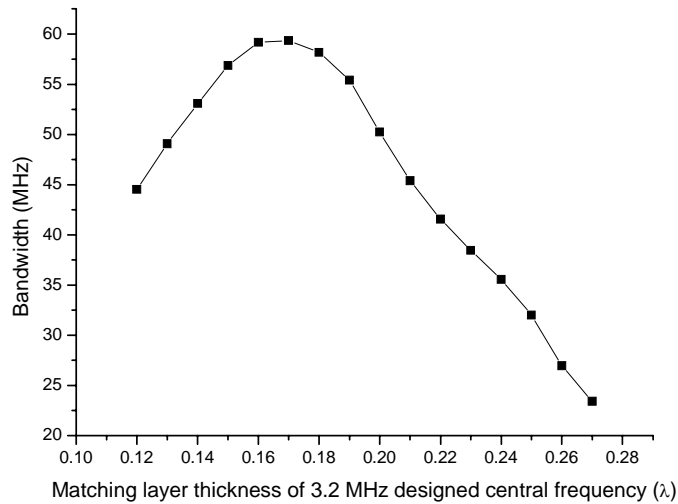
Figure 3.6 Simulated transducer's bandwidth with different thicknesses of the matching layers.

Taking a transducer designed with a center frequency of 3.2 MHz as an example, we may find that the optimized thickness of the matching layer is not at the 1/4 wavelength. Actually, the bandwidth curve reaches its peak at 0.17λ (here λ is the wavelength at 3.2 MHz). Transducer's bandwidth increases from 30% with 0.25λ matching to about 60% with 0.17λ matching. This is a great improvement for transducer performance, and also means that the quarter λ matching does not always work well for transducer design. The simulation result seems to be confusing, since it conflicts with

the conventional quarter λ matching models. But it can be easily understood from the

center frequency shift view point.
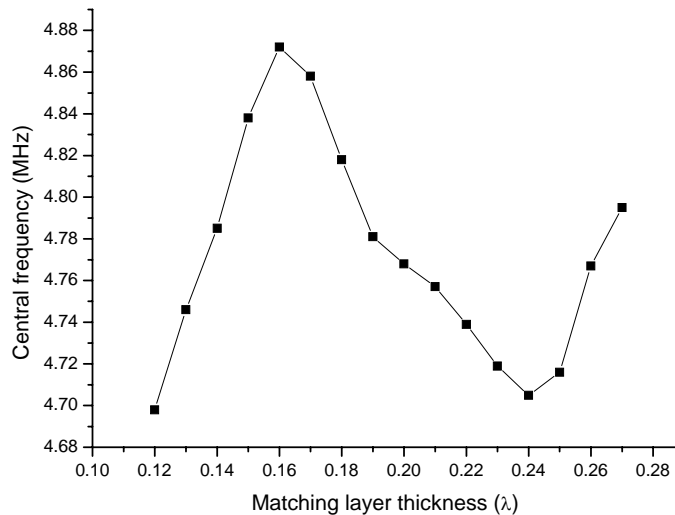
Figure 3.7 Simulated center frequency with different thicknesses of the matching layers.

As we mentioned above, the center frequency of the transducer will shift with

different fabrication parameters, including the thickness of the matching layer. We

found that, if we add double quarter matching layers onto the transducer designed for

3.2 MHz center frequency, the final center frequency should reach as high as 4.7 MHz,

not 3.2 MHz any more. So actually the quarter wavelength matching at 3.2 MHz could

not serve well for this 4.7 MHz center frequency transducer. However, when we reduce

the matching layers' thickness to 0.17 wave length at 3.2 MHz, actually we shift the

transducer center frequency to 4.86 MHz. Now the 0.17 wave length at 3.2 MHz

matching is just about 1/4 wavelength at 4.86 MHz. Arguing from this view, the quarter

matching theory still works well in our simulation results. There is no conflict between

the simulation result and matching theory.

3.2.3   Effective Coupling Factor Optimization

In transducer simulation, there is a constant called effective coupling constant, k_{eff},

which can be calculated using the following formula:

$$k_{eff} = \frac{\sqrt{f_a^2 - f_r^2}}{f_r}, \tag{3.9}$$

where this effective coupling constant determines transducer bandwidths. The square of

the coupling factor is proportional to the partitioning of the energy available in the

electrical domain over that in the mechanical domain, or vice versa. Also, theoretical

analysis has shown that the ultimate bandwidth available from a transducer design is

proportional to k_{eff}^2. Here we will check the possibility of the broad bandwidth PMN-PT

single crystal transducer, based on the improvement of the effective coupling factor of

the active material – PMN-PT single crystal.
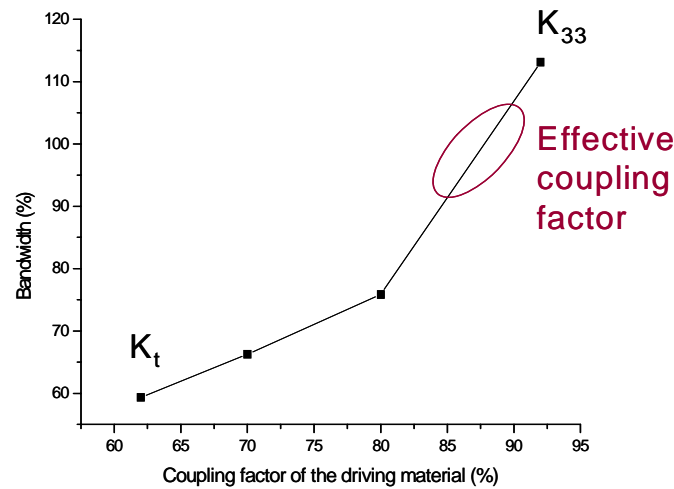
Figure 3.8 Simulated transducer's bandwidths with different coupling factors.

We use different coupling factor in our transducer simulation, with optimized matching system to check the improvement of the effective coupling constant's effect on the transducer performance — the transducer bandwidth. Input parameters on x axis range from 62% to 93% (PMN-PT single crystal's k_t to its k_{33}). The simulation results look impressing. The highest bandwidth when PMN-PT single crystal works with its k_{33}, could be as high as 110%. Of course the active element of PMN-PT single crystal will not work on its bar mode (the k_{33} mode), since the structure of the phased array is some kind of 2-2 composite, and the effective coupling constant should be between the thickness mode and bar mode. Judging from the curve above, if we want a transducer with bandwidth over 100%, the k_{eff} needs to be in the scale of the circled area, around 85% with the same matching and backing system. Also this study gives us a clue about

how to improve the transducer's performance besides of the matching and backing used in the transducer. Attempts to improve the active element's effective coupling factor will be discussed later.

In this simulation study, we have focused on the tailored matching scheme for PMN-PT single crystal, which has lower acoustic impedance compared to PZT ceramic. The double matching scheme of 6.0/2.1 MRayls with optimized thickness of 0.17λ at 3.2 MHz was chosen as the best of all acoustic matching system on a 3.0 MRayls light backing. With the improved electromechanical coupling factor of PMN-PT single crystal, there is the possibility of improving the transducer's bandwidth to over 90%. For even broader bandwidth, heavy backing is another good choice which could increase the transducers' bandwidth dramatically on sacrificing the transducer's sensitivity.

3.2.4   Double $\lambda/8$ Matching Scheme

The PMN-PT phased array transducer with over 90% bandwidth from our simulation results is acceptable compared to the 70% bandwidth commercial PZT transducers. Research from other paper gives similar result, for example the 2.6 MHz PMN-PT phased array transducer from Humanscan with 91.5% bandwidth [Rhim et. al, 2002].

Our further study of the acoustic design shows that there is a new approach to increase the transducer's bandwidth, i.e. the double λ/8 matching system. Graded or multilayer (>2 layers) matching scheme can further improve the performance of the transducer [Edmiston et. al, 2005; Shohei et. al, 2002; Felix et al, 2001], but it will also add significant cost and complexity in fabrication process. But theoretically, two λ/8 matching layers may also be suitable for the acoustic matching for broadband transducers.

Our simple understanding for the λ/8 matching scheme is that, the double λ/8 matching layers provide a taped quarter matching layer for the low frequency signal, at f; while for the high frequency signal, around 2f, each λ/8 matching layer is just a quarter-wavelength matching for the 2f signal. By providing improved transmission efficiencies for both low frequency (f) and high frequency (2f) signals, the bandwidth of the transducer with double λ/8 matching can be even broader than the conventional two quarter wavelength matching transducer. Simulation results with different thicknesses of the matching layers are plotted in Figure 3.9 with both light backing and heavy backing.
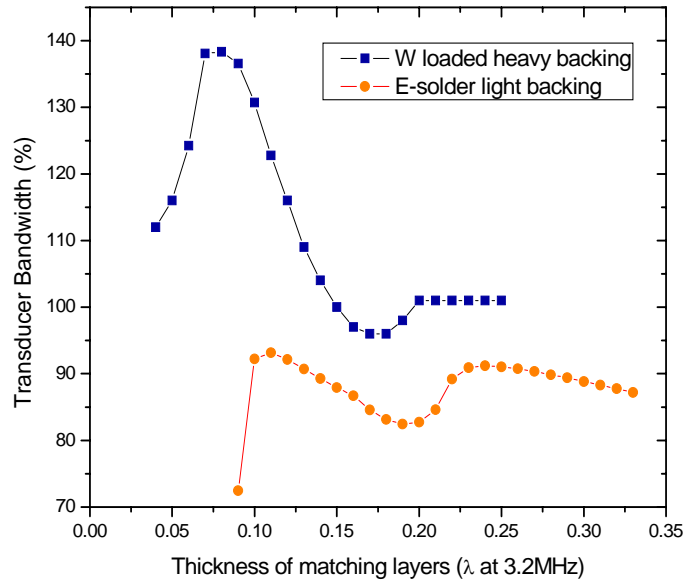
Figure 3.9 Simulation result of the transducer's bandwidth with different matching thicknesses on light and heavy backings.

According to the simulation results, with a light backing (acoustic impedance of 5.9 MRayls), there is still a peak at 0.10λ matching thickness, but there is no significant improvement of the transducer bandwidth (increase from 90% to 95%). While for the transducer with tungsten loaded heavy backing (acoustic impedance of 12.5 MRayls), the peak of the bandwidth curve reaches up to 140% under optimized simulation parameters. This result proves the theory of the double 1/8λ matching scheme. The advantage for λ/4 match is the larger process window for matching layer thickness, even the maximum bandwidth is only 95%. Though the highest bandwidth is 140% for λ/8

matching, the disadvantage is the narrow process window, where very accurate thickness control of the matching layers is needed in fabrication process.

3.3   Summary

In this chapter, we used PiezoCAD to simulation the work performance of PMN-PT single crystal transducer. Starting from the base-line of the acoustic scheme of a high performance PZT transducer, the effects of backing, effective acoustic impedance of PMN-PT, thickness of the matching layers and effective coupling factor to the transducer performance have been studied separately. Including all these factors, the acoustic impedance of the backing materials, and the thickness of the matching layer show great effect to the transducer's performance. A novel double $\lambda/8$ matching scheme is also proposed to further increase the transducer's bandwidth, and the result shows great improvement.

Based on the simulation result above, two prototype transducers with optimized double $\lambda/4$ matching layers and double $\lambda/8$ matching layers, respectively, were fabricated and characterized. Details of the fabrication techniques and characterization results were introduced in the next chapter.

CHARPTER 4

TRANSDUCER FABRICATION AND CHARACTERIZATION RESULTS

Based on the modeling results, two PMN-PT phased array transducers (namely quarter-wavelength matching and 1/8 wavelength matching transducers) have been fabricated and characterized. In this chapter, detailed fabrication processes in making these two transducers and the characterization results, as well as simulation results, of these two fabricated transducers are introduced.

4.1 PMN-PT Single Crystal Processing

Electrode Coating and Poling

The single crystal is (001)-cut PMN-28%PT fabricated by the Shanghai Institute of Ceramics. The PMN-PT sample was first cut into the desired dimensions, lapped down with sand papers to the designed thickness and polished with 12.5 μm alumina powder (BUEHLER) to form a smooth surface. The crystal was then subsequently deposited

with Cr/Au electrode on both surfaces with DC magnetron sputtering at room

temperature. The depositions of Cr/Au are performed at power of 70 W, and the

deposition time for Cr is 1 min and 10 min for Au. The thickness of the electrode layer

is about 300 nm determined by surface profiler. PMN-PT sample was then poled in

silicone oil at 120℃ with 1 kv/mm electric field for 10 min. Impedance analyzer

(Model HP 4294) and d_{33} meter were used to measure the k_t (k_t was calculated with the

Equation (3.8) introduced in Chapter 3) and d_{33} of the PMN-PT sample. Density and

sound velocity were also measured to get the acoustic impedance of PMN-PT single

crystal. A typical PMN-PT sample's impedance spectrum is shown in Figure 4.1 with f_a

=7.1 MHz and f_r=5.8 MHz. Some measured PMN-PT single crystal characteristics used

in transducer fabrication were listed in Table 4.1.

Table 4.1 Measured PMN-PT single crystal properties.

Density	8100 kg/m^3
Longitude velocity	3600 m/s
Acoustic impedance	29 MRayls
d_{33}	1200 pC/N
K_t	0.63
Clamped dielectric constant	1380
Loss	0.008

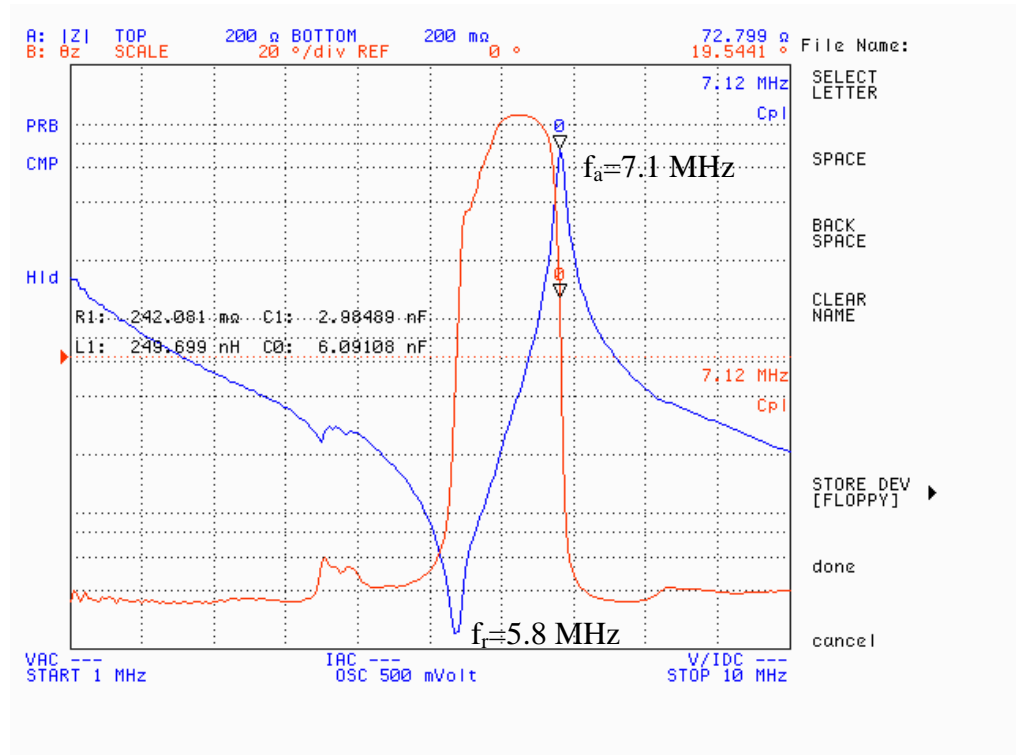Figure 4.1 PMN-PT single crystal impedance spectrum.

Temperature-dependent Dielectric Spectrum and P-E Loops

The temperature-dependent relative permittivity curve of the poled PMN-PT single crystal sample upon heating is shown in Figure 4.2. From the relative permittivity curve, the Curie temperature T_c is determined to be 134 ℃ at which the ferroelectric to paraelectric phase transition takes place.
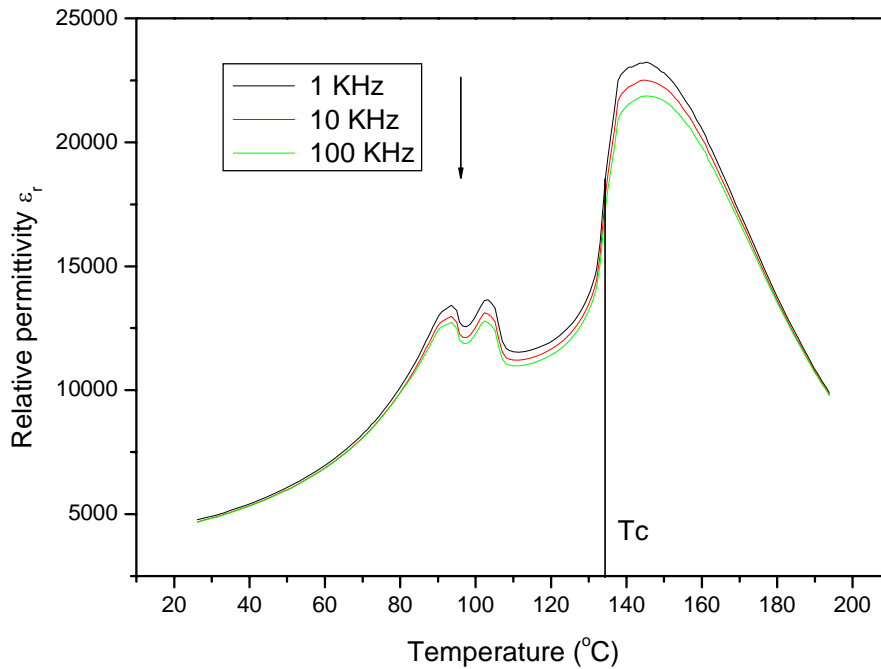
Figure 4.2 Temperature-dependent relative permittivity curves for poled (001)-cut
PMN-28%PT single crystal upon heating.

The P-E loops of the PMN-PT sample at different temperatures and the temperature-dependent P_r are shown in Figure 4.3. One can see that the depoling phenomenon happens when the sample is at 60℃ above. Therefore, the temperature in the fabrication process should be well controlled below 60℃ to eliminate the single crystal performance decrease due to depoling. Otherwise, repoling after the transducer fabrication needs to be performed.

Figure 4.3 Temperature dependence of hysteresis loops and remnant polarization
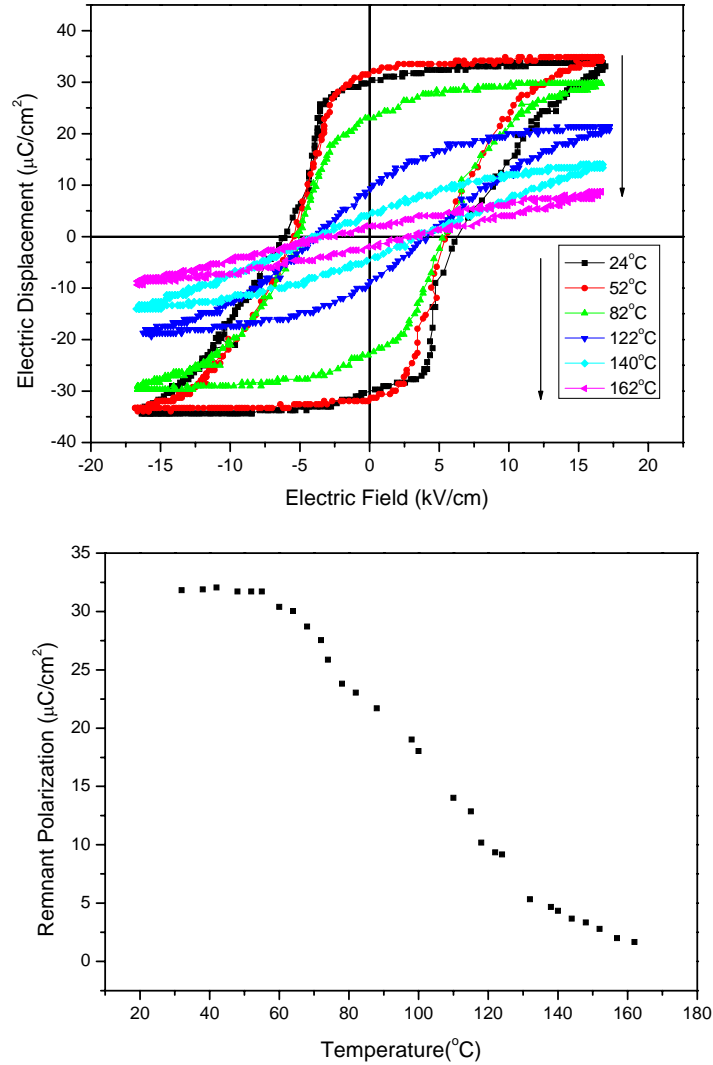for (001)-cut PMN-28%PT single crystal.

Dicing and Size Effects

In order to optimize the crystal dicing speed and understand the size effect to the

coupling factor, the crystal has been cut into different width slices followed by

impedance and d_{33} measurements. In our experiment, the crystal with size of $26 \times 13 \times$

0.33 mm^3 was diced on DISCO DAD321 dicing machine to different element widths

with blade NBCZ 2050. Rotation speed is 40000 rpm, and its feeding speed is well

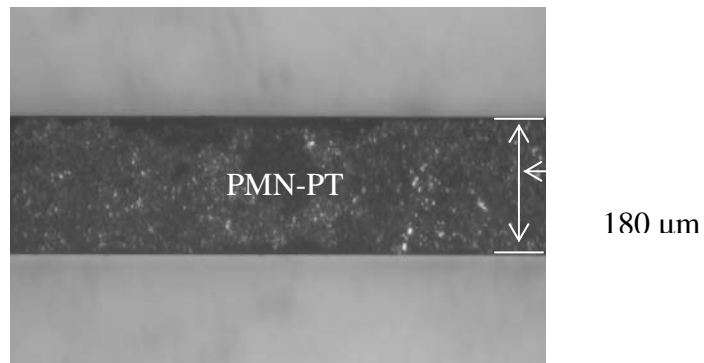controlled at 0.4 mm/s for safety.

PMN-PT

180 um

Figure 4.4 Diced element of PMN-PT single crystal.

One single element diced from PMN-PT slice is shown in Figure 4.4. It can be

seen that there is no damaged edge, suggesting that the blade and dicing parameters

were appropriate for PMN-PT single crystal.

For different widths of the diced crystal samples, d_{33} and k_t were measured in order

to check the effect of the size and the dicing impact to the PMN-PT single crystal

properties. The measured data are listed in Table 4.2, and it is apparent that, as the width

decreases, the electromechanical coupling factor k_{33}' increases from 63% to 81%. With

smaller element width, the aspect ratio of the PMN-PT element is bigger, so the

vibration mode of the element would be more closer to the pure bar mode. This means

that the element's effective electromechanical coupling factor k_{33}' would be more closer

to k_{33} (0.92). We chose 0.18 mm element width (its aspect ratio is about 0.55 with 0.33

mm element thickness) in our prototype to provide better effective electromechanical

coupling factor and small cross talk between neighbor elements for our phased array.

However, drop of the piezoelectricity is also found from d_{33} measurement result. This

may be due to the stress and heat introduced crystal depoling in the dicing process,

which deserve further detailed study.

Table 4.2 Properties of the diced PMN-PT single crystal elements.

Element width (mm)	d_{33} (pC/N)	k_{33}'
26	1200	0.63
0.22	1000	0.73
0.20	1000	0.76
0.18	1000	0.81

4.2 Transducer I:

Quarter Wavelength Matching Transducer

4.2.1 Backing and Matching

In order to prepare passive materials (including backing and matching) with

desired acoustic properties, epoxy and metal powder composite is a suitable choice.

Low viscosity epoxy is proved to work fairly well for powder distribution from our

experimental results. We chose low viscosity epoxy, Araldite LY 564/Aradur 2954, as

the epoxy matrix, and tungsten powders as the additive to prepare heavy backing for the

PMN-PT transducer.

To prepare the epoxy material, Araldite LY 564 and hardener Aradur 2954

(HUNTSMAN) was mixed at 100: 35. The mixture was stirred and vacuumed for about

5 min to push the bubbles generated in the interaction up to the mixture's surface.

Tungsten powders with designed weight were added into the above epoxy. The mixture

was then stirred and placed in a vacuum chamber for about 30 min to get the air bubbles

out from the mixture. The composite was then cured at air pressure overnight and 60℃

for 6 hours, followed by the last lapping and polishing steps. Figure 4.5 is a SEM image

of the tungsten powders embedded in epoxy matrix, where it can be seen that tungsten

powders distribute homogeneously and form a suitable passive backing material.
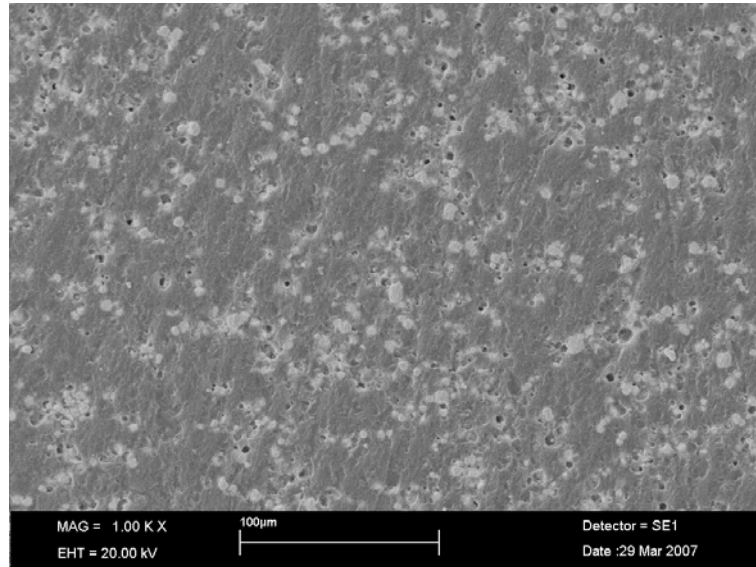
Figure 4.5 SEM image of epoxy-tungsten composite.

For matching materials, Epoxy 7-2316 was chosen due to its high temperature curing property, so we could have more time for additive mixing when we work at room temperature. Alumina powders were first mixed with Epoxy 7-2316 at designed weight ratio. The mixture was then placed onto a flat surface, heated up to 80℃ (the temperature when Epoxy 7-2316 has the lowest viscosity) and vacuumed for about 30 min. The sample was then cured at 90℃ for two days and then lapped down from the top surface and polished for the following characterizations.
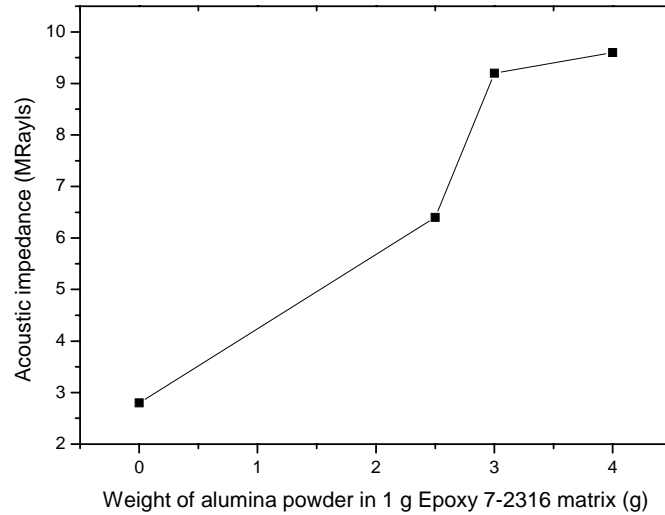
Figure 4.6 Variation of composites' acoustic impedances with the weight of alumina
mixed with 1 g Epoxy 7-2316.

With the help of decreased viscosity of the Epoxy 7-2316 after having been heated

to 80 ℃, weight fraction of the alumina can reach as high as 80%. Several samples with

different weight ratios were prepared. The samples' acoustic impedances are from 6.4 to

9.6 MRayls from our experimental results. They are suitable candidates for acoustic

matching materials for PMN-PT transducers. Properties of the backing, first matching

and second matching materials used in transducer I were list in Table 4. 3.

Table 4.3 Acoustic properties of passive layers for λ/4 matching transducer.

Matrix	Additive	Weight proportion	Use	Density (kg/cm^3)	Sound velocity (m/s)	Acoustic impedance (MRayls)
Epoxy 7-2316	Alumina powder	1:0	Second matching	1.1	2500	2.8
		1:2.5	First matching	2.4	2700	6.4
Araldite LY 564	Tungsten powder	1:8	Backing	6.0	1700	10.2

4.2.2 Transducer Installation Process

The cured Epoxy 7-2316 sample was lapped down and polished with 2000 # sand paper to the designed thickness of 200 μm as the second matching layer. As for the first matching layer, the alumina powder/Epoxy 7-2316 mixture was lapped down and polished to the thickness of 220 μm. The thicknesses of both matching layers are the optimized results from the PiezoCAD simulation of double quarter matching scheme. Tungsten powder and Araldite LY 564 mixture was polished to a flat surface with thickness about 10 mm (for adequate attenuation) as the backing layer for the transducer.
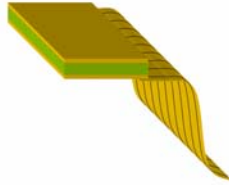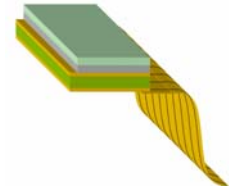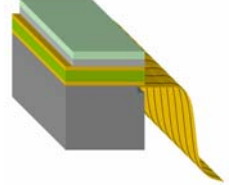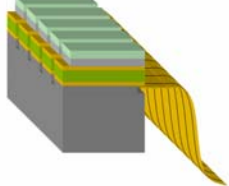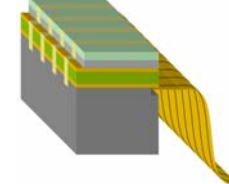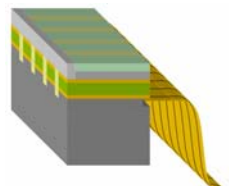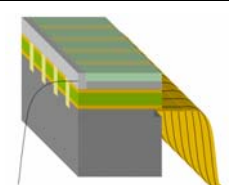
Flexible circuit with 150 μm gold wire arranged with a constant pitch of 0.26 mm was connected to one edge of the PMN-PT sample with silver epoxy EE 1-924 and

cured at 50 ℃ overnight. The second matching layer, first matching layer, PMN-PT

single crystal layer and the backing layer were then bonded together with M-bond 610

epoxy under external pressure to provide a thin bonding line and cured at 50 ℃

overnight. The multilayer stack was then diced on DISCO dicing machine, aliened with

the Au metal line on the flexible circuit. The element pitch is 0.26 mm, and the kerf

width is 0.08 mm. Dicing depth is 1.05 mm (0.3 mm into the backing substrate) to

eliminate the cross-talk between neighboring elements.   Detailed fabrication steps are

listed in Table 4.4. Photo of the finished phased array transducer is shown in Figure 4.7.

Table 4.4 Phased array fabrication steps.

|	
Au/Cr electrode was deposited onto both surfaces. The sample was then poled in silicone oil.	
Flexible circuit was connected to the bottom electrode with conductive epoxy.	
The double matching layers with designed thicknesses were bonded onto the front surface of the PMN-PT sample one by one.	
Backing with a flat surface was bonded to the back surface of the PMN-PT sample.	
Dicing step was performed on the stack to form separated array elements along the golden wire on the flexible circuit.	
Filler was then filled into the dicing kerfs	
Conductive epoxy was used to connect every element on the top electrode	
After the ground wire was connected to the silver epoxy, the prototype is ready for characterization.	
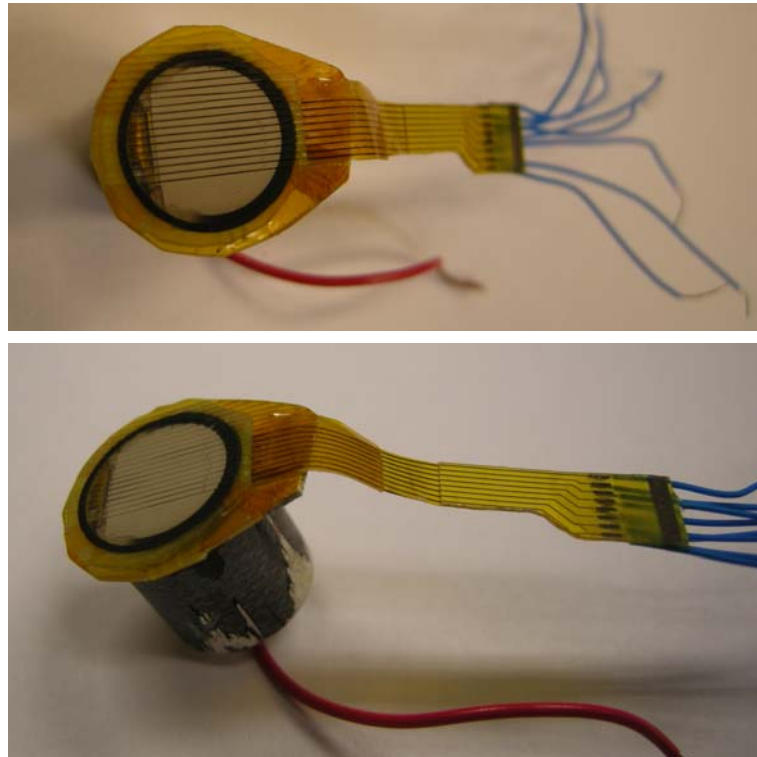
Figure 4.7 Picture of the λ/4 matching phased array PMN-PT transducer.

4.2.3 Transducer Performance Evaluation
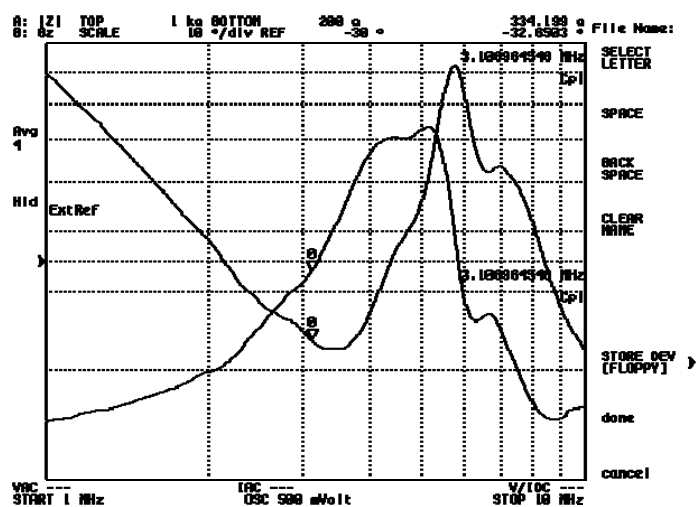
Figure 4.8 Impedance spectrum of the λ/4 matching transducer element.

The diced phased array elements were first tested on HP 4294A impedance

analyzer for their impedance spectrum, which is shown in Figure 4.8. Resonant peak at

3.5 MHz and anti-resonant peak at 5.7 MHz can be identified from the impedance

spectrum and the effective coupling factor k_{33}' can be calculated to be 81% from

equation (3.8).

The phased array PMN-PT transducer was then characterized in a

sound-absorption water tank at room temperature. A polished stainless steel flat plate

was placed 20 mm (the focal length of the transducer) away from the transducer front

surface, normal to the transducer maximum response axis to reflect the ultrasound pulse

back to the transducer. A standard pulse/receiver (Panametrics, Model 5900PR) was

used under the conditions of energy = 16 μJ, damping resistance = 50 Ω, gain = 26 dB,

and attenuation =26 dB.   There are 16 elements fabricated on this transducer. Most

elements work well in our experiments. Choosing the element with the best

performance, Figure 4.9 gives the ring-down waveform measured in the pulse echo

response and its Fourier transform of this received time-domain echo response.

Transducer performance characterization results including bandwidth and center

frequency are listed in Table 4.5.
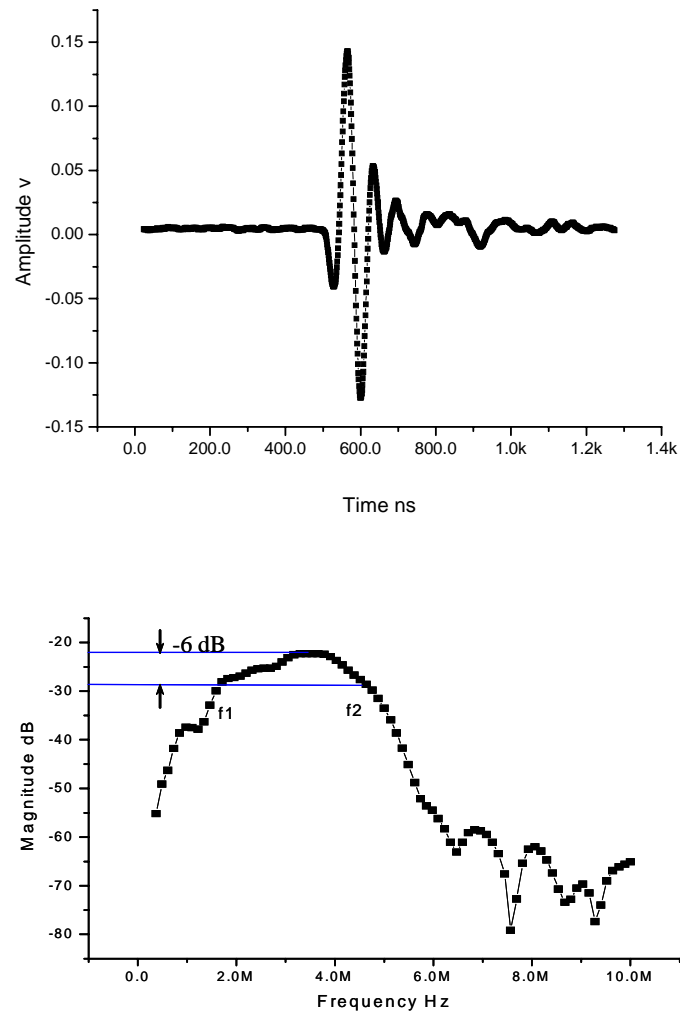
Figure 4.9 Pulse echo response and frequency spectrum of the λ/4 matching
phased array transducer.

Table 4.5 Phased array λ/4 matching transducer parameters.

f_r	f_a	Center frequency	Fractional bandwidth	Relative sensitivity
1.7 MHz	4.6 MHz	3.2 MHz	92%	-43dB
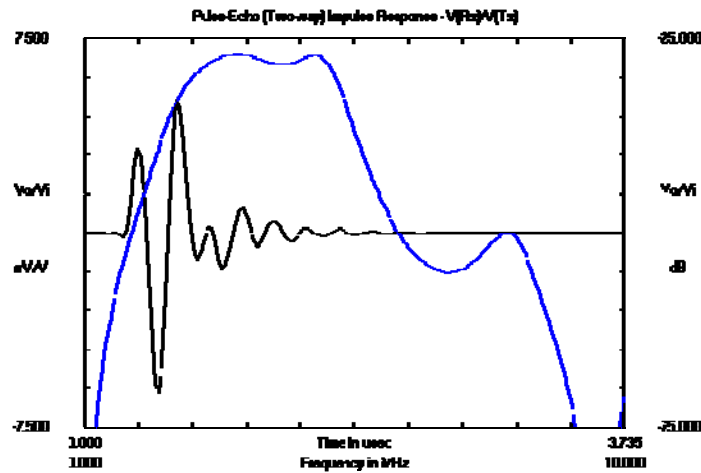
Figure 4.10 PiezoCAD simulation results of λ/4 matching transducer.

Given the parameters of the backing, matching and the PMN-PT active element, the PiezoCAD simulation provides us the predicted waveform and bandwidth spectrum of the transducer, as shown in Figure 4.10. The center frequency of the transducer is at 3.27 MHz and the bandwidth is 95%.

The center frequency of the fabricated transducer is 3.2 MHz, matches well with our design. The 92% bandwidth of the transducer is acceptable, but is still a litter narrower than the simulation result which is 95%. The reason might be caused by the preciseness of the sound velocity of the first matching layer. As we know that the lamination phenomenon always happens in the powder-epoxy mixture. We prepared a thick slice matching material for sound velocity measurement, and then lapped it down

to quarter wavelength according to the measured sound velocity of the thick matching material sample. Actually, the lamination might change the acoustic properties of the matching layer used in the transducer. The error of the sound velocity of the matching layer makes its thickness depart from the real quarter wavelength, and thus may affect the transducer's performance.

4.3   Transducer II:
1/8 Wavelength Matching Transducer

According to the double 1/8 wavelength matching scheme proposed in Chapter 3. Another PMN-PT transducer with double λ/8 matching layers was fabricated in the pursuing of even broader bandwidth compared to transducer I with conventional double quarter wavelength matching. This work was done in the Resource Center for Medical Ultrasonic Transducer Technology in the University of Southern California, as the oversea attachment program for research students in the Hong Kong Polytechnic University, under the supervision of Prof. K.K. Shung and Dr. Q.F. Zhou.

4.3.1   Backing and Matching

The PMN-PT single crystal sample with a dimension of $5 \times 13 \times 0.33$ mm^3 were coated with 300 nm Au/Cr electrode and poled in air at $120℃$. Flexible circuit with 150 μm gold wire arranged with a constant pitch of 0.26 mm was connected to one edge of

the PMN-PT sample with E-solder 3022 and cured at room temperature overnight.

Silver particles and Insulcast 501 were mixed at weight ratio of 3:1.25, vacuumed for

about 3 min and transferred onto the front surface of the PMN-PT single crystal with a

thin layer of adhesion promoter AP131. The PMN-PT sample was then put into Alegra

6 centrifuge (BECKMAN COULTER) with mixture on it, centrifuged at 3000 rpm for

15 min and cured overnight at room temperature. This silver/epoxy composite cast on

the PMN-PT single crystal will serve as the first matching layer of the transducer. It was

then lapped down and polished with 12.5 μm alumina polishing powder (BUEHLER) to

the optimized thickness of about 47 μm according to PiezoCAD simulation with double

λ/8 matching scheme introduced in chapter 3. Then EPO-TEK 301 was vacuumed to get

rid of the bubbles, then cast and cure at room temperature overnight, on the surface of

the first matching layer. This EPO-TEK 301 will serve as the second matching layer of

the transducer. After the curing of EPO-TEK 301, it is lapped down to the thickness of

57 μm according to the PiezoCAD optimization. Mixture of tungsten powder and

EPO-TEK 301 was vacuumed for 30 min and cured overnight. The composite was then

polished to a flat surface with thickness of about 10 mm as the backing layer for the

transducer. Acoustic properties of these three layers are listed in Table 4.6.

Table 4.6 Acoustic properties of passive layers for λ/8 matching transducer.

Matrix	Additive	Weight proportion	Use	Density (kg/cm^3)	Sound velocity (m/s)	Acoustic impedance (MRayls)
EPO-TEK 301			Second matching	1.1	2600	3.0
Insulcast 501	Silver particles	1:2.5	First matching	3.8	1900	7.3
EPO-TEK 301	Tungsten powder	1:10	Backing	7.4	1700	12.5

The backing layer was then bonded onto the back surface of the PMN-PT single

crystal layer with EPO-TEK 301 and adhesion promoter AP131, under external pressure

to provide a thin bonding line and cured at room temperature overnight. The multilayer

stack was then diced with Thermocarbon TCAR864-1 dicing saw, aligned with the

golden line on the flexible circuit. Rotation speed of the blade is 36000 rpm and the

feeding speed is 0.4 m/s. With a 0.070 mm dicing blade, the kerf width between

neighbor elements is about 0.080 mm. The dicing depth is 0.730 mm (about 0.3 mm

into the backing substrate) to eliminate the cross-talk between neighboring elements.

The following steps are similar with those of the quarter λ matching transducer listed in

Table 4.4, and will not be introduced in detail.

4.3.2   Transducer Performance Evaluation

A representative phased array elements' impedance spectrum measured on HP

4294A impedance analyzer is shown in Figure 4.11. It can be identified that the

resonant peak (f_r) is at 2.5 MHz, and anti-resonant peak (f_a) is at 3.8 MHz. The effective

coupling factor is calculated to be 79% from Equation (3.8). There is also a low

resonant peak next to the thickness vibration resonance from the impedance spectrum.

This is the planar mode resonation after the f_a on thickness mode, which is caused by

the low aspect ratio of the PMN-PT elements. The presence of the planar vibration

mode may affect the transducer's performance by coupling the vibration energy into

unwanted vibration mode.
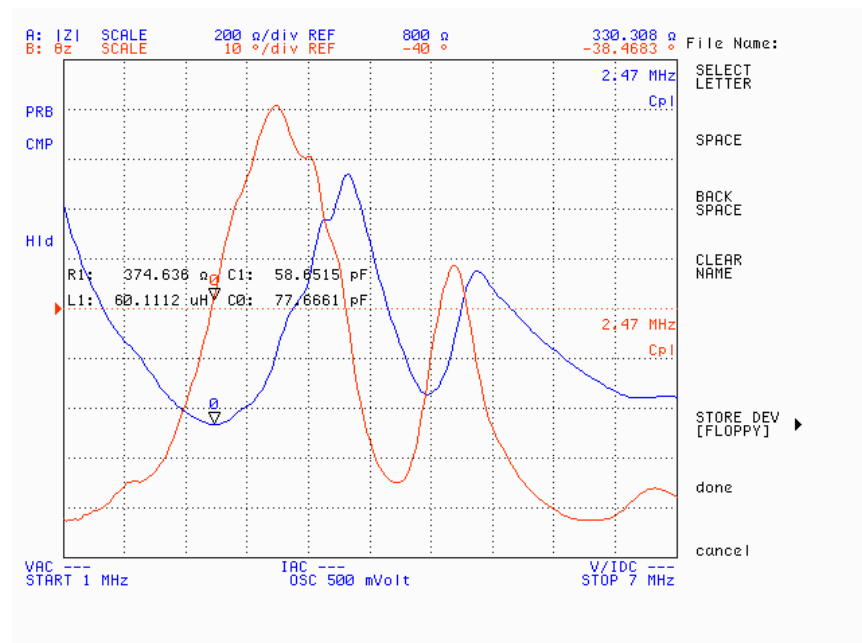
Figure 4.11 Impedance spectrum of the λ/8 matching transducer element.

This phased array PMN-PT transducer was then characterized in a sound

absorption water tank at room temperature. A flat quartz plate was placed 20 mm (the

focal length of the transducer) away from the transducer front surface, normal to the

transducer maximum response axis to reflect the ultrasound pulse back to the transducer.

A standard pulse/receiver (Panametrics, Model 5900PR) was used under the conditions

of energy = 1 μJ, damping resistance = 50 Ω, gain = 26 dB, and attenuation =26 dB.

There are 16 elements fabricated on this transducer. Most elements work well in our

experiments. Choosing the element with the best performance, Figure 4.12 gives the

ring-down waveform measured in the pulse echo response and its Fourier transform.

Transducer performance characterization results including bandwidth and center

frequency are listed in Table 4.7.
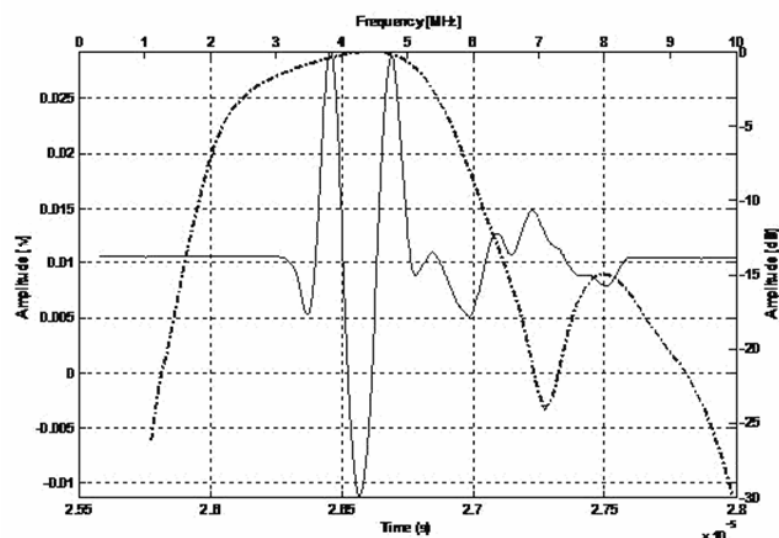
Figure 4.12 Frequency spectrum of the λ/8 matching phased array
transducer.

Table 4.7 Phased array λ/8 matching transducer parameters.

f_r	f_a	Center frequency	Fractional bandwidth	Relative sensitivity
2.0 MHz	5.6 MHz	3.8 MHz	96%	-48dB

Given the parameters of the backing, matching and the PMN-PT active element, the PiezoCAD was used to simulate the pulse-echo waveform and bandwidth spectrum of transducer II, as shown in Figure 4.13. The center frequency is determined to be 3.4 MHz and the bandwidth is 120%.
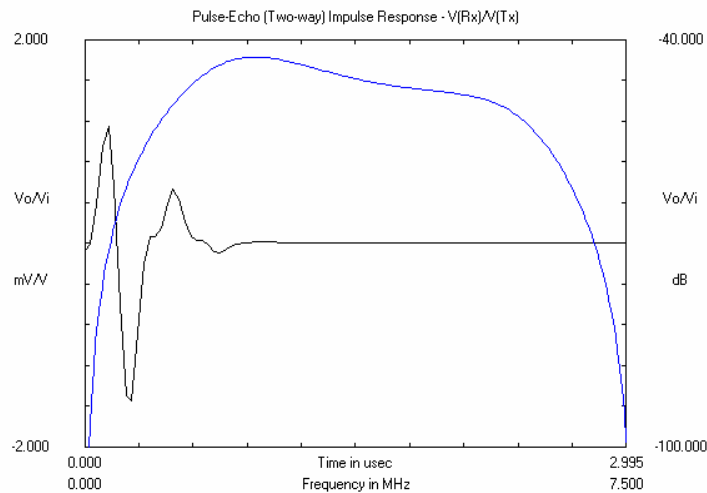
Figure 4.13 PiezoCAD simulation results of λ/8 matching transducer.

The center frequency of the λ/8 matching transducer is 3.8 MHz, which is higher than the simulated results 3.4 MHz. The bandwidth of the fabricated transducer is 96%,

which is not as high as the120% bandwidth from the simulation results. From the

frequency spectrum, we can find that the high frequency signal sensitivity is better than

low frequency signal part, not as shown in the simulation results in which the sensitivity

of the low frequency part is higher in contrast. The center frequency also shifts to the

higher frequency side. This might be due to the acoustic mismatch of the double 1/8

wavelength matching layers for the low frequency signals. Here, the double 1/8

wavelength matching layers are expected to work as one quarter-wavelength matching

with taped acoustic impedance. While this simply taped matching layer dose not work

as efficient as expected, thus causes the low sensitivity in the low frequency part, and

therefore makes the bandwidth decrease in low frequency part and the center frequency

shift to higher frequency. Nevertheless the 96% bandwidth still show trend of

improvement compared to the conventional quarter-wavelength matching scheme

transducer. Further study of the $\lambda/8$ matching scheme should be taken to insure the

simulated results of over 100% bandwidth, including the fabrication processing, and

improvement of the effective coupling factor of the PMN-PT element by varying the

element aspect ratio and etc.

Here in the prototype II, the mechanism of its double $\lambda/8$ matching scheme is to

serve for both low and high frequency signals on sacrificing the transmission efficiency

of the signal on the center frequency. We can find that the transducer's sensitivity drops for about 5 dB from the measured result, compared to the former quarter-wavelength matching single crystal transducer. The high coupling factor of PMN-PT single crystal is assumed to achieve higher sensitivity compared to conventional PZT transducers. So this sensitivity decrease is acceptable from the design point for broad-bandwidth property of the single crystal transducers.

4.4   Summary

Based on the simulation with the help of PiezoCAD, two PMN-PT phased array transducers, with $\lambda/4$ and $\lambda/8$ matching layers, were fabricated successfully. Both transducers show 90% above bandwidth (92% and 96%, respectively), which is a big increase compared to the conventional PZT phased array transducers (about 70%). The simple substitution of the PZT ceramic with PMN-PT single crystal that has higher electromechanical coupling factor as the active element in ultrasound transducer, can improve the transducer performance dramatically.

Compared to the well-accepted double quarter wavelength matching system, the novel double $\lambda/8$ matching scheme shows a trend to further improve the bandwidth of the transducer from my research. Although, in my experiment, the improvement of the transducer bandwidth is not as large as predicted, the measured results do show the

trend of the bandwidth enlargement and center frequency shift as predicted in the

simulation. Further study of the λ/8 matching mechanism and transducer fabrication

techniques is needed beside of this thesis's work.

CHAPTER 5

CONCLUSION AND
FUTURE WORK

In this thesis work, modeling, fabrication and characterization of low frequency (about 3 MHz) phased array medical imaging ultrasound transducers using PMN-PT single crystal have been carried out, and the following results have been achieved.

PiezoCAD has been carried out to simulate the performance of PMN-PT single crystal transducer. Starting from the base-line of the acoustic scheme of a high performance PZT transducer, the effects of backing, effective acoustic impedance of PMN-PT, thickness of the matching layers and effective coupling factor to the transducer performance have been studied separately. The results show that all these factors, including the acoustic impedance of the backing material, and the thickness of the matching layer show great effect to the transducer's performance. A novel double $\lambda/8$ matching scheme, besides of the quarter wavelength matching, is proposed to

further increase the transducer's bandwidth, and the simulation results show great improvement.

In my study, based on the simulation result above, two prototype transducers with optimized double $\lambda/4$ matching layers and double $\lambda/8$ matching layers, respectively, were fabricated and characterized. Both transducers show 90% above bandwidth (92% and 96%, respectively), which is a big increase compared to the conventional PZT phased array transducers (about 70%). The substitution of the PZT ceramic with PMN-PT single crystal with higher electromechanical coupling factor, as the active element in ultrasound transducer, can improve the transducer performance.

Compared to the well-accepted double quarter wavelength matching system, the novel double $\lambda/8$ matching scheme shows a trend to further improve the bandwidth of the transducer, with a bandwidth of about 96%, from my research. Although, in the experiment, the improvement of the transducer bandwidth is not as large as predicted, the measured results do show the trend of the bandwidth enlargement and center frequency shift as predicted in the simulation. Further study of the $\lambda/8$ matching mechanism and transducer fabrication techniques is needed in addition to this thesis's work.

Further improvement of the prototype may be done by improving the coupling

factor of the active material. 1-3 composite is suitable not only in single element transducers but also in low frequency phased array transducers. The k_{33} for 1-3 PMN-PT composite, which is as high as 93%, can increase the bandwidth of the transducer over 20% from simulation result. Attempt of using the 1-3 PMN-PT composite as the active elements in phased array transducers has been tackled in my work (not included in thesis), and should be studied in future work of this thesis.

REFERENCES

Bjørn A.J. Angelsen, "Ultrasound Imaging: Waves, Signals, and Signal Processing", Trondhejm, Norway : Emantec, 2000.

Charles E. Baumgartner, David M. Mills, "Acoustic Backing Material for Small-Element Ultrasound Transducer Arrays", US Patent, Pub. No.: US 2005/0127793.

Jonathan M. Cannata and K. Kirk Shung, "A Comparison of Model and Experiment for a High Frequency (35 MHz) Linear Ultrasonic Array." 2003 IEEE Ultrasonics Symposium, 1658-1662.

Jonathan M. Cannata, "High Frequency (>20 MHz) Ultrasonic Arrays for Medical Imaging Applications", Doctor of Philosophy Thesis, The Pennsylvania State University, 2004.

Jie Chen, Rajesh Panda, "Realizing Dramatic Improvements in the Efficiency, Sensitivity and Bandwidth of Ultrasound Transducers", Pure Wave Crystal Technology White Paper, Philips, 2004.

Jie Chen and Rajesh Panda, "Review: Commercialization of Piezoelectric Single Crystals for Medical Imaging Applications", 2005 IEEE Ultrasonics Symposium, 235-240.

Rick Edmiston, "Triple Quarter-Wave Transducer Designs", www. STI-Ultrasound.com, 2005.

Kenneth R. Erikson, Francis J. Fry and Joie P. Jones, "Ultrasound in Medicine—A Review", IEEE Transactions on Sonic and Ultrasonics, Vol. su-21, No. 3, July 1974, 144-170.

Nicolas Felix, Leong Ratsimandresy and Rémi Dufait, "High Bandwidth, High Density Arrays for Advanced Ultrasound Imaging", 2001 IEEE Ultrasonics Symposium, 1123-1126.

Ruo Fen, Zhongjin Yao, Xunli Guan et. al, "Ultrasound Handbook", Nanjing University Press, 2001.

Emanuel J. Gottlieb, Bruce Lai, Xiaochen Xu, Jonathan Cannata, Jesse Yen, Qifa Zhou, Pengdi Han, Hossein Ameri, Tanapat Ratanapakorn, Aaron Barnes, Mark Humayun, K. T.R. Grurraja and Rajesh K. Panda, "Current Status and Future Trends in Ultrasonic Transducers for Medical Imaging Applicaions", ISAF 98, Proceedings of the Eleventh IEEE International Symposium, Applications of Ferroelectrics, 223-228.

Emanuel J. Gottlieb, Jonathan M. Cannata, Chang Hong Hu, K. Kirk Shung, "Development of a High-Frequency (>50 MHz) Copolymer Annular-Array Ultrasound Transducer", IEEE Transactions on Ultrasonics, Ferroelectrics, and Frequency Control, Vol. 53, No. 5, May 2006, 1037-1045.

Wesley Hackenberger, Paul W. Rehrig, Timothy Ritter, and Thomas Shroout, "Advanced Piezoelectric Materials for Medical Ultrasound Transducers", 2001 IEEE Ultrasounics Symposium, 1101-1104.

Wesley Hackenberger, Xiaoning Jiang, and Paul Rehrig, Xuecang Geng, Alan Winder, Flemming Forsberg, "Broad Band Single Crystal Transducer for Contrast Agent Harmonic Imaging ", 2003 IEEE Ultrasounics Symposium, 778-781.

Wayne R. Hedrick, David L. Hykes, Dale E. Starchman, "Ultrasound Physics and Instrumentation", St. Louis : Mosby, 1995.

Yasuharu Hosono, Kouichi Harada, Senji Shimanuki, Shiroh Saitoh, and Yohachi Yamashita, "Crystal Growth and Mechanical Properties of Pb[(Zn1/3Nb2/3)0.91Ti0.09]O3 Single Crystal Produced by Solution Bridgman Method", Japanese Journal of Applied Physics, 1999, 38, 5512-5515.

J. Kuwata, K. Uchino, S. Nomura, "Dielectric and Piezoelectric Properties of 0.91Pb(Zn1/3 Nb2/3) O3-0.09PbTiO3 Single Crystals", Japanese Journal of Applied Physics,1982, 21, 1298-1302.

Ronald E. Mckeighen, "Optimizing Transducer Design for Medical Imaging", Engineering in Medicine and Biology Society, 1989, 11TH Annual International Conference, 402-404.

Ronald E McKeighen, "Design Guidelines for Medical Ultrasonic Arrays", Proc. SPIE Medical Imaging 1998, Vol. 3341, 2-18.

Stéphane Michau, Pascal Mauchamp, Rémi Dufait, "Single Crystal-based Phased Array for Transoesophagial Ultrasound Probe", 2002 IEEE Ultrasonics Symposium Proceedings,   1269-1272.

X. Ming Lu, T. L. Proulx, "Single Crystals vs. PZT Ceramics for Medical Ultrasound Applications", 2005 IEEE Ultrasonics Symposium, 227-230.

C.G. Oakley, M.J. Zipparo, "Single-crystal Piezoelectrics: A Revolutionary Development for Transducers", 2000 IEEE Ultrasonics Symposium Proceedings, 1157–1167.

S. Park and T. Shrout, "Characteristics of Relaxor-based Piezoelectric Single Crystals for Ultrasonic Transducers", IEEE Transation on Ultrasonics, Freeoelectrics and Frequency Control, Vol.44, 1140-1147, 1997.

H.W. Persson and C. H. Hertz, "Acoustic Impedance Matching of Medical Ultrasound Transducers", Ultrasonics. 1985 Mar, 23(2), 83-9.

Ratsimandresy. L, Mauchamp. P, Dinet. D, Felix. N, Dufait. R, "A 3MHz Two Dimensional Array based on Piezocomposite for Medical Imaging." 2002 IEEE Ultrasonics Symposium, 1265-1268.

S. Rhee, T.A. Ritter, K.K. Shung, H. Wang, W, Cao, "Materials for Acoustic Matching in Ultrasound Transducers", 2001 IEEE Ultrasonics Symposium, 1051-1055.

Sung Min Rhim, Ho Jung, Seduk Kim, and Sang-Goo Lee, "A 2.6 MHz Phased Array Ultrasonic Probe Using 0.67Pb(Mg1/3Nb2/3)O3-0.33PbTiO3 Single Crystal Grown by The Bridgeman Method", 2002 IEEE Ultrasonics Symposium, 1143-1148.

T. A. Ritter, X. Geng, K. K. Shung, P. D. Lopath, S.-E. Park, and T. R. Shrout, " Single Crystal PZN-PT Polymer Composite for Ultrasound Transducer Aplications," IEEE Transactions on Ultrasonics, Ferroelectrics and Frequency Control, vol. 47, 792-800, 2000.

Saitoh, S. Takeuchi, T. Kobayashi, T. Harada, K. Shimanuki, S. Yamashita, Y. "A 3.7 MHz Phased Array Probe Using0.91Pb(Zn1/3Nb2/3)O3-0.09PbTiO3", IEEE Transactions on Ultrasonics, Ferroelectrics and Frequency Control, Vol. 46, No. 2, 414-421, Mar. 1999.

Shohei Sato, Hidetsugu Katsura, and Kazuhiro Kobayashi, "Experimental Investigation of Phased Array Using Tapered Matching Layers", 2002 IEEE Ultrasonics Symposium, 1235-1238.

K. Kirk Shung, "PMN-PT High Frequency Ultrasonic Needle Transducers for Pulsed Wave Doppler in the Eye", 2005 IEEE Ultrasonics Symposium, 2227-2230.

Siemens Medical Solutions Ultrasound Division, "A Closer Look at Four-dimensional Imaging Capabilities with Premium Performance Ultrasound Systems", Business Briefing: Women's Healthcare 2004.

Dave Waller, Jie Chen, and T.R Gururaja, "Requirements of Piezoelectric Materials for Medical Ultrasound Transducers", ISAF '96: Proceedings of the Tenth IEEE International Symposium on Applications of Ferroelectrics, 565-568.

Haifeng Wang, Tim Ritter, Wenwu Cao, and K. Kirk Shung, "Passive Materials for High-frequency Ultrasound Transducers", Proceedings of SPIE, Medical Imaging Symposium, Vol. 3664, 35-42, 1999.

Q.Q. Zhang, F.T. Djuth, Q.F. Zhou, C.H. Hu, J.H. Cha, K.K. Shung, "High Frequency Broadband PZT Thick Film Ultrasonic Transducers for Medical Imaging Applications", Elsevier B. V. Ultrasonics 44, 2006, 711-715.

R. Zhang, B. Jiang and W. Cao, "Elastic, Piezoelectric and Dielectric Properties of Multi-domain 0.67Pb(Mg1/3Nb2/3)O3-0.33PbTiO3 Single Crystal", Journal of Applied Physics, vol. 90, 3471-3475, 2001.